Influence of fluvial environments on sediment archiving processes and temporal pollutant dynamics (Upper Loire River, France)

E. Dhivert, C. Grosbois *, S. Rodrigues, M. Desmet

Université François Rabelais de Tours, EA 6293 GéHCO, Parc de Grandmont, 37200 Tours, France

HIGHLIGHTS

- Divergence on long-term evolution of sedimentary pollution archived in a floodplain.
- Archiving capacity depends on the connection degree to the river channel.
- Archived geochemical signals depend on sampling statutes in the floodplain.
- Good resolution on short-time variations of pollution in the paleochannel.
- Pollution trend altered by redistribution processes in the floodplain ridge.

ARTICLE INFO

ABSTRACT

Floodplains are often cored to build long-term pollutant trends at the basin scale. To highlight the influences of depositional environments on archiving processes, aggradation rates, archived trace element signals and vertical redistribution processes, two floodplain cores were sampled near in two different environments of the Upper Loire River (France): (i) a river bank ridge and (ii) a paleochannel connected by its downstream end. The base of the river bank core is composed of sandy sediments from the end of the Little Ice Age (late 18th century). This composition corresponds to a proximal floodplain aggradation (<50 m from the river channel) and delimits successive depositional steps related to progressive disconnection degree dynamism. This temporal evolution of depositional environments is associated with mineralogical sorting and variable natural trace element signals, even in the <63-μm fraction. The paleochannel core and upper part of the river bank core are composed of fine-grained sediments that settled in the distal floodplain. In this distal floodplain environment, the aggradation rate depends on the topography and connection degree to the river channel. The temporal dynamics of anthropogenic trace element enrichments recorded in the distal floodplain are initially synchronous and present similar levels. Although the river bank core shows general temporal trends, the paleochannel core has a better resolution for short-time variations of trace element signals. After local water depth regulation began in the early 1930s, differences of connection degree were enhanced between the two cores. Therefore, large trace element signal divergences are recorded across the floodplain. The paleochannel core shows important temporal variations of enrichment levels from the 1930s to the coring date. However, the river bank core has no significant temporal variations of trace element enrichments and lower contamination levels because of a lower deposition of contaminated sediments and a pedogenetic trace elements redistribution.

© 2014 Elsevier B.V. All rights reserved.

1. Introduction

The grain size distribution of alluvial deposits controls the fluvial architecture and fine-grained sediments, essentially settling in out-of-channel forms (Walling et al., 1998; Bridge, 2003; Houben, 2007). Because metallic and organic contaminants are typically associated with the finest particles during sediment transport, floodplains play a key role in pollutant cycles, constituting short- to long-term storage areas for contaminated sediments (Bradley and Cox, 1990; Martin, 2000; Heaven et al., 2000; Lecce and Pavlowsky, 2014). Therefore, floodplains are often cored to study pollutant temporal trends and to identify temporal variability of natural and anthropogenic sources (*e.g.*, Grosbois et al., 2012 for the Loire Basin (France) and neighboring hydrosystems: Grousset et al., 1999 for the Garonne Basin; Gocht et al., 2001; Berner et al., 2012 for the Rhin basin; Le Cloarec et al., 2011 for the Seine basin; Ferrand et al., 2012; Desmet et al., 2012; Mourier et al., 2014 for the Rhone basin). However, floodplains cannot be considered to be a homogenous depositional environment because of (i) the temporal variability of aggradation rates caused by long-term evolutions of natural

* Corresponding author. Tel.: +33 247367002.
E-mail address: cecile.grosbois@univ-tours.fr (C. Grosbois).

and anthropogenic influences on parameters controlling sediment deposition (Hoffmann et al., 2010; Hughes et al., 2010; Meitzen et al., 2013; Grygar et al., in press) and (ii) the short-term (overbank floods) and the short-space (lateral transect) scale variability of aggradation rates, sediment textures and storage capacities (Nanson and Croke, 1992; Walling et al., 1997; Walling and He, 1998; Lecce and Pavlowsky, 2004; Rodrigues et al., 2006; Baborowski et al., 2007; Dieras et al., 2013). This short-scale variability of sediment inputs influence contamination levels and archived temporal dynamics of pollutants (Bradley and Cox, 1990; Birch et al., 2001; Martin, 2000; Heaven et al., 2000; Baborowski et al., 2007; Bábek et al., 2008; Grygar et al., 2010; Vrel et al., 2013; Hostache et al., 2014). Additionally, between morphological units of a floodplain, large differences may exist in the nature and degree of post-depositional processes managing the fate of archived pollutants. Archived contaminated sediments can be remobilized during erosion episodes (Macklin and Klimek, 1992; Lecce and Pavlowsky, 1997; Förstner et al., 2004; Lecce and Pavlowsky, 2014). A high spatial variability exists during high discharge events of erosion intensity across floodplains (Benedetti, 2003, Fuller, 2008; Dieras et al., 2013; Thompson and Croke, 2013). Additionally, exchanges between particulate and dissolved fractions inside the sedimentary column are an important factor managing the fate of archived contaminants. These exchanges can be controlled by organic matter degradation and seasonal variations of redox potential, which affect morphological units of floodplains differently (van Griethuysen et al., 2005, Charriau et al., 2011, Schulz-Zunkel et al., 2013). The vertical redistribution of contaminated particles can occur in floodplain soils where pedogenic activity has been settled (Fujikawa et al., 2000; Palumbo et al., 2000).

These variability factors question the representation at the basin scale of pollutant temporal dynamics archived in a punctual situation of a floodplain. In other words, what are the conditions allowing the building of representative pollutant trends from a floodplain core? In this study, the influence of depositional environments on sediment archiving processes, aggradation rates and associated trace elements (TE) was investigated at a local scale in the Upper Loire River floodplain. The aim was to highlight mechanisms controlling the archiving of sediments and associated TE and the temporal dynamics of contaminants in two floodplain cores sampled in two different morphological units separated by less than 50 m: (i) a ridge of the river bank and (ii) a paleochannel connected at its downstream end (Fig. 1).

2. Study area and methods

2.1. Main characteristics of the study area

The Loire River basin (117,800 km² –1013 km long) is among the ten largest W-European basins and is the largest in France (Fig. 1a). The Decize station is located in the upper reach of the Loire River (14,752 km² –450 km long), 30 km upstream of the Allier River
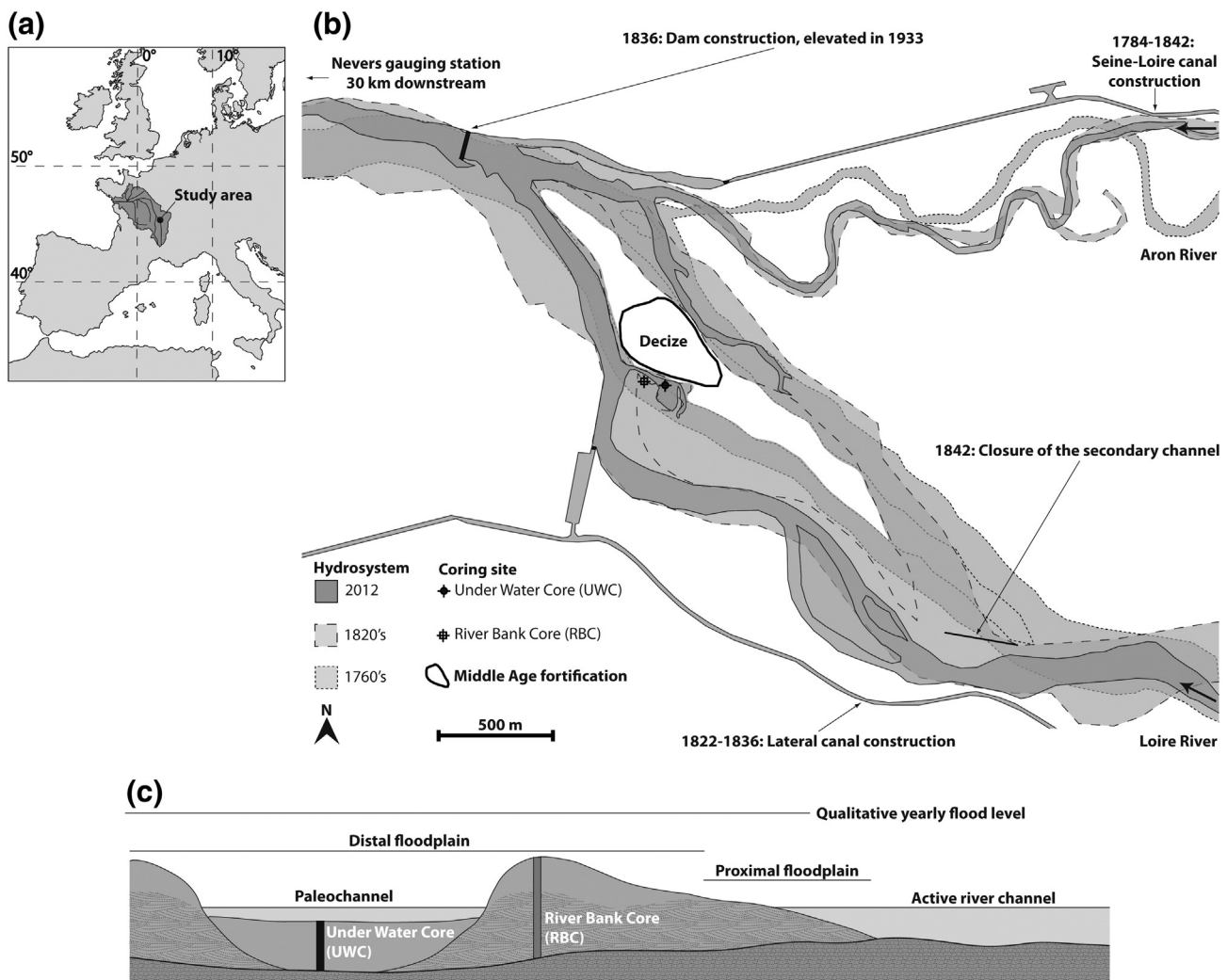

Fig. 1. a — Location of the study area in W-Europe, b — morphodynamic history, hydrosystem anthropization and local industrial histories of the study area (data from www.geoportail.fr, 2014; Decize Municipal Archive, 2014), and c — schematic view of the sample strategy.

confluence. This station is located close to the confluence with the Aron tributary, the Loire River lateral canal and the Seine-Loire canal. Because of the Decize dam, built in 1836 and elevated in 1933 (Fig. 1), the main channel of the Loire River allows the shipping connection between these canals. The coring site (46°49′36.6″N, 3°27′38.2″E) is located 1.5 km upstream from this dam and 400 m downstream from the maximum dam influence (the lock of the lateral canal).

The geology of the Upper Loire Basin is different. According to the French geological survey, the upstream region of the Loire hydrosystem essentially drains granites, gneisses and micaschists from the eastern region of the French Central Massif, an old massif inherited from the Variscan orogeny (480–290 Ma), However, two other geological units constitute bedrocks of the Upper Loire Basin: i) a volcanic area from the Tertiary as the basin head of the Loire River and ii) sedimentary basins from the Carboniferous and Oligocene–Miocene (mainly sandstones, marls and clays).

The hydrology of the upper basin is influenced by a balance of oceanic and Mediterranean rainfall during autumn and winter, completed by snow-melt in spring (Dacharry, 1974). The annual hydrological cycle of the Upper Loire River, at the Nevers gauging station (30 km downstream of the coring site), is characterized by a high flow period from November to May. Monthly discharges calculated over 59 years range from 199 $m^3 \cdot s^{-1}$ to 323 $m^3 \cdot s^{-1}$. Low flow occurs in summertime with average values ranging from 50 $m^3 \cdot s^{-1}$ to 121 $m^3 \cdot s^{-1}$ (data from www.hydro.eaufrance.fr). At this gauging station, the 50-year flood peak discharge reached 2200 $m^3 \cdot s^{-1}$ (daily discharge), 1900 $m^3 \cdot s^{-1}$ for the 20-year flood, 1700 $m^3 \cdot s^{-1}$ for the 10-year flood, 1400 $m^3 \cdot s^{-1}$ for the 5-year flood and 1000 $m^3 \cdot s^{-1}$ for the 2-year flood. Four catastrophic flood events occurred in the basin after the water depth measurement began at the Decize dam gauging station (1836): 1846 (7.1 m), 1856 (6.5 m), 1866 (7.4 m) and 1907 (6.3 m) (www.centre.developpement-durable.gouv.fr; www.vigicrues.fr).

The studied floodplain results from a lateral migration of a relatively straight channel, which was active until the 18th century, to the present meander. This sinuosity was initiated at the end of the Little Ice Age (LIA), between the 1760s and 1820s, and was associated with channel widening (Fig. 1b). This morphological evolution was described for a large number of fluvial systems all over the world (e.g., Arnaud-Fassetta, 2003; Landon, 1999 for the Rhône River; Knox, 2006 for the Upper Mississippi River) and even in the Upper Loire River for a historical meander located 10 km upstream of the study area (Leteinturier et al., 2000; Babonaux, 1970). These rapid changes in the river channel planform are attributed to a large sedimentary transport resulting from combined actions of important flood events associated with climate change of the end of the LIA and soil erosion magnification by human land use. Additionally, river bed modifications (embankments, dams, hydraulic structures for water-depth control), performed since the 19th century along the Loire River, triggered a narrowing of the main river channel, its incision and the development of woody vegetation (Gasowski, 1994; Rodrigues et al., 2006; Détriché et al., 2010; Latapie, 2011; Grivel and Gautier, 2012; Macaire et al., 2013; Latapie et al., 2014). Presently, the study area corresponds to a typical point bar complex characterized by a ridge and swale topography delimiting former scroll bars. Bridge (2003) proposes a definition of point bar and scroll bar concepts by explaining that sediments are preferentially deposited in the inner part of meanders, allowing sedimentary bars to form with a scroll planform shape. The lateral migration of the river channel induces the formation of successive bars and establishes a point bar complex. In the study area, the paleochannel, which is flooded throughout the year, constitutes a remnant of the initial channel and is preserved by anthropogenic actions.

2.2. Analytical method

The two sediment cores were sampled in May 2012, after the last spring floods. The underwater core (UWC), was sampled in the deepest area of the paleochannel (Fig. 1c). The top of the sedimentary infill was elevated at 189.8 m asl, under 0.5 m of water column on the coring date. A UWITEC gravity corer fitted with a 2 m long and 90 mm diameter plastic liner was used for the UWC. The river bank core (RBC), was sampled on the adjacent river bank (Fig. 1c), 48 m E–S–E from the UWC at the top of the closer ridge, elevated at 191.3 m asl. For this core, an Eijkelkamp mechanical percussion corer equipped with 1 m long and 63 mm diameter plastic liners was used.

Material and methods used for this study are detailed in Dhivert et al. (in press). All of the analyses were performed with 2 cm-slices of core sediments. To complement visual and textural descriptions of sedimentary units, temporal variations of deposition conditions were reconstructed using the C–M diagram (Passega, 1957, 1964) and specific segments were understood following universal pattern interpretations (Bravard et al., 2014; Arnaud-Fassetta, 2003; Bravard and Peiry, 1999). The rolling domain (N–O domain, Fig. 2) was anchored in the Loire River context using bed load sediments sampled more than 30 km downstream of the study area (Valverde et al., 2013). Bed load sediments involve a broad spectrum of particles (D_{50} range between 1.3 mm and 15.0 mm) from coarse sands (1–2 mm) to medium gravels (8–16 mm). A grain size measurement was performed on fresh sediments using a laser diffraction microgranulometer (Mastersizer 2000, Malvern) as it is the only method to establish sedimentological patterns and destroy a minimum amount of material. For poorly sorted sediments, the grain size distribution of the coarsest particles must be considered carefully (Pye and Blott, 2004). Similar to Dhivert et al. (in press), the replicability was low for the ninety-ninth percentile of very poorly sorted fine-grained layers. The ninetieth percentile (D_{90}) was used as the C parameter to be more representative of the coarsest grain size, and the M value corresponded to the median grain size (D_{50}).

Regarding the structural differences between the UWC (aquatic sediments saturated) and the RBC (terrestrial sediments showing a secondary porosity), age-models were designed to calculate mass accumulation rates (MAR, $kg \cdot m^{-2} \cdot year^{-1}$; Van Metre et al., 2004) to correct coring compaction. MARs are calculated, dividing cumulative dry mass (cum; $kg \cdot m^{-2}$) between each date-bounded by time intervals. The dry mass parameter (DM; $kg \cdot m^{-2}$) is calculated as follows:

$$DM = (1-n) \cdot DS \cdot Th \tag{1}$$

where n represents the porosity (%) corresponding to the volume of water in a well with a known volume of sediments (here $2.4 \cdot 10^{-5}$ m^3) and is calculated from the weight difference between the fresh and dried sediments. DS is the apparent density of sediments ($g \cdot m^{-3}$) corresponding to the dry mass material in the defined volume and Th the thickness of the sampled layer (here $2.0 \cdot 10^{-2}$ m). The age of sediments (Date) at level i is calculated as follows from the top of the core (2012 in this study as the coring date) to the first time marker:

$$Date_i = coring \, date - cum_i / MAR. \tag{2}$$

For sediment layers j, which is older than the first time marker i, Eq. (3) is then applied:

$$Date_j = marker \, date_i - \left(cum_j - cum_i \right) \Big/ MAR_j. \tag{3}$$

Absolute dating was based on ^{137}Cs artificial radionuclide vertical distribution. ^{137}Cs measurements were performed using gamma spectrometry with very low-background detectors, coaxial HP Ge N-type (8000 channels, low back-ground).

Geochemical analyses were performed on the <63 μm fraction. The 190–202 cm deep layer was pooled because <63 μm material was too low. Analyses were made at the SARM-CRPG laboratory (http://helium.crpg.cnrs-nancy.fr/SARM). Material was completely digested with $LiBO_2 - Li_2B_4O_7$ on a tunnel oven and placed in an acidic solution
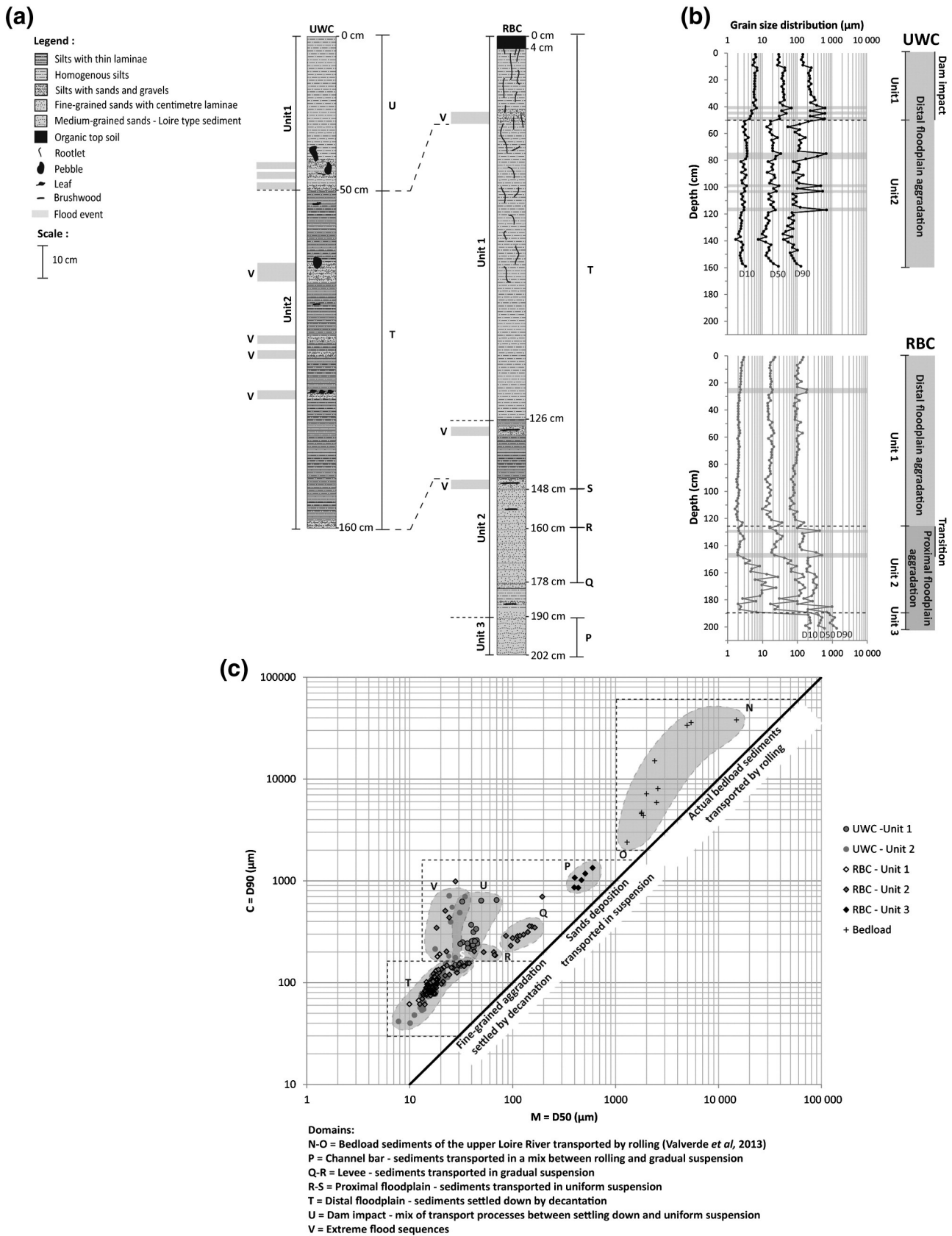
Fig. 2. a — Logs description, b — grain size distribution, and c — temporal evolution of settling conditions characterized with the C–M diagram (Passega, 1957, 1964).

before being analyzed by ICP-OES (ICap 6500, Thermo Scientific) for total major and minor element concentrations, and ICP-MS (Thermo Elemental X7, Thermo Scientific) for trace elements, except for Hg, which was completed using DMA-80 (Milestone). The total organic carbon (TOC), after an HCl attack and total sulfur (TS), was analyzed by O_2 flow combustion at 1350 °C with a SC 144-DRPC (Leco). The analytical

error tacking into account accuracy of digestion processes and analyses was within 1% for major elements and 10% for trace elements.

3. Results and discussion

3.1. Archiving processes during the floodplain edification

3.1.1. Aggradation processes in the floodplain

The texture of sediments can be used as proxy for tracing the geomorphological evolution of the floodplain and the associated aggradation processes accompanying the river bank accretion and the lateral migration of the river channel (Bravard et al., 2014; Passega, 1957, 1964).

The RBC core presents two distinct sequences: the deepest sequence (126–202 cm) rich in sand (>63 μm) and the upper sequence (0–126 cm) composed of fine-grained sediments (<63 μm; Fig. 2a). According to Walling et al. (1997) and Walling and He (1997), during overbank floods, sandy sediments are deposited in the highly connected context of a proximal floodplain (within the first 50 m from the river channel) and fine-grained sediments settle in the lowly connected context of a distal floodplain. In this study, this distinction allows for the characterization of two large depositional environments with specific aggradation processes over space and through time (Fig. 2b).

The proximal floodplain sequence, archived at the base of the RBC (126–202 cm), presents a general fining upward (r = 0.6, p < 0.05, n = 33, Fig. 2b, Table 1). This is confirmation of a connection degree evolution during the aggradation period.

The deepest unit of the RBC (190–202 cm), named unit 3 (Fig. 2a), is composed of moderately sorted sands (Table 1). Compared to actual bed sediments with high grain size variability (N–O domain), unit 3 draws the P domain in the C–M diagram (Fig. 2c). This sedimentary layer can be interpreted as channel bar sediments fed by a mix between rolling and gradual suspension. It marks the first step of point bar formation as defined by Nanson and Page (1983).

Unit 2 (Fig. 2a) of the RBC (126–190 cm) is characterized by a high variability of grain size distribution delineating four progressive steps of proximal floodplain evolution. The 178–190 cm deep layer is very heterometric (composed of fine-grained sediments) and alternates with heterometric sandy layers (Table 1). This sub-unit has an erratic pattern in the C–M diagram and does not materialize specific domain. This high retention capacity of fine and coarse sediments is related to a vegetated filter effect (Rodrigues et al., 2007; Euler et al., 2014). The upper sub-unit (160–178 cm; Fig. 2a) is composed of fine-grained sands (Table 1). This sedimentary layer is in the Q–R domain on the C–M diagram (Fig. 2c) and is characterized by a distribution parallel to the C = M line. Sediments were transported by graded suspension and deposited in a levee. These first two sub-units (178–190 cm and 160–178 cm) highlight the point bar accretion process during lateral migration of the river channel. The two next sub-units (148–160 cm and 126–144 cm deep) are composed of finer grained sediments. The interval at 148–160 cm deep is made of a balanced proportion of fine-grained sands and fine-grained sediments (Table 1). In this layer, the M value varies by 56% without a specific bottom-up trend but the C value stays constant. It is located in the R–S domain in the C–M diagram (Fig. 2c). Sediments were transported by uniform suspension during overbank floods and constituted a proximal top river bank aggradation. The last interval of unit 2 (126–144 cm; Fig. 2a) is a centimeter laminated and composed of fine-grained sediments (Table 1). here is less of a sandy fraction than in the sub-unit (148–160 cm), which is mainly represented by very fine-grained sands. This sub-unit transitions between uniform suspension and another domain, noted T in the C–M diagram (Fig. 2c), where fine-grained sediments settled during long inundation periods. These two last intervals correspond to a higher disconnection degree aggradation. The river bank begins to be too high or/and too far from the river channel to be regularly submerged by high-energy and turbulent flows transporting sediments by gradual suspension.

Sediments of the upper unit of the RBC (0–126 cm), noted unit 1 (Fig. 2a) and corresponding to the distal floodplain aggradation, are uniformly composed of fine-grained sediments (Table 1). The sand fraction is low and largely composed of very fine-grained sands. This sedimentary unit fully constitutes domain T in the C–M diagram (Fig. 2c). Up to 80 cm deep, the exponential bottom-up increase of the TOC content combined with the relative abundance of roots and the apparent secondary porosity are evidence of soil formation. The 4 last centimeters correspond to a saturated organic top soil (water content > 87%; TOC > 3.5%).

The 160 cm long record of the UWC represents the entire column of fine-grained sediments settled in the paleochannel. The 2 last centimeters (158–160) contain heterometric sands and constitute the interface with the initial floor of this sedimentary trap. Two depositional processes occurred during the sedimentary infilling, corresponding to two sedimentary units (Fig. 2a).

The deepest unit of the UWC (Unit 2; 50–160 cm) is faintly laminated and has a texture comparable to the uppermost unit of the RBC (Table 2) This unit 2 is included in the same domain T of the C–M image as is the upper sequence of the RBC (Fig. 2c) aggraded by the settling of fine-grained sediments.

The upper unit of the UWC (Unit 1; 0–50 cm) is significantly different from unit 2, i.e., a lack of laminations and a lesser abundance of fine-grained sediments (Table 2). The sandy fraction is mainly composed of fine-grained sands. Unit 1 is located in domain U in the C–M image (Fig. 2c), presenting coarser sediments when compared with the T domain. The aggradation of this unit results from a mix of settling of fine-grained sediments and uniform suspension of fine-grained sands. In this study, the Decize Dam was severely elevated in 1933 to increase river channel depth at the lateral canal lock. Because of this, another sedimentary process initiated and affected the UWC. The dam elevation may have induced slackwater deposition of fine-grained sands in the paleochannel by its downstream connection during high discharge levels.

As shown by Walling and He (1997) for surface sediments, long-term depositional processes are mainly influenced by the distance to the main river channel and, in a lesser way, the connection degree and floodplain topography. Low spatial and temporal variability of sediment textures inside the distal floodplain constitute a key point to sample representative sedimentary archive. However, topography, such as local river planform changes, must be accounted for to understand sedimentary transitions, as the low topographic areas are more influenced by connection degree variations.

3.1.2. Extreme flood sequences as proxy of the archiving capacity

The last domain defined in the C–M diagram, noted V (Fig. 2c), is characterized by a significant increase of C values, and stable M values. The V domain gathers layers enriched in heterometric sands with centimeter pebbles (Fig. 2a, Tables 1 and 2). These layers are well recorded in the UWC at 114–118 cm, 102–104 cm, 98–100 cm, 74–80 cm, 48–50 cm, 44–46 cm and 40–42 cm. However, they are not well preserved in the RBC (present at 24–28 cm in the distal floodplain aggradation). RBC flood layers are also visible at 144–148 cm, 128–130 cm, corresponding to high energy inputs of sands (proximal floodplain aggradation; Fig. 2a).

Microfacies of archived extreme flood sequences can be related to observations from Walling et al. (1997), which highlights increasing grain sizes for the coarsest particles in contemporaneous flood deposits.

Even if the settling conditions are similar in the UWC and the RBC before dam elevation, why there are no flood sequences preserved in the RBC during distal floodplain aggradation?

In natural topographic depressions, such as abandoned channels (UWC), extreme flood records are described as sandy units composed of coarser particles than sediment deposited during standard overbank floods (Bábek et al., 2011; Werritty et al., 2006). The remobilization of trapped sediments is low in these former channels, even during

Table 1

Selected major and trace element concentrations in the <63 µm sediments according to depth, Cs activity, median grain size (D_{50}) and percentages of sands (63 µm–2 mm), silts (2–63 µm) and clays (<2 µm) in the bulk sediment layers of the river bank core (RBC). n.d. = not determined; <d.l. = below the detection limit.

Depth (cm)	Age (y)	^{137}Cs (Bq/kg)	D50 (µm)	Sand (>63 µm) (%)	Silt (2–63 µm) (%)	Clay (<2 µm) (%)	Si (%)	Al (%)	TOC (%)	S tot. (%)	Hf (ppm)	As (ppm)	Bi (ppm)	Cd (ppm)	Cr (ppm)	Cu (ppm)	Hg (ppm)	Mo (ppm)	Ni (ppm)	Pb (ppm)	Sb (ppm)	Sn (ppm)	U (ppm)	W (ppm)	Zn (ppm)
0–2	2012	7 ± 0.6	23.0	25	69	6	26.5	7.3	4.0	0.08	10.9	27.9	1.3	1.0	123.1	32.1	0.195	1.1	39.7	72.0	2.1	20.6	9.2	6.5	196.1
2–4	2010	n.d.	20.5	22	72	6	26.7	7.5	3.6	0.05	11.0	29.8	1.3	1.3	129.2	35.8	0.250	1.1	38.7	77.0	2.3	22.4	10.1	6.9	201.0
4–6	2001	n.d.	17.0	20	74	7	26.9	7.7	3.5	0.06	10.4	31.3	1.4	1.2	131.9	37.5	0.270	1.2	40.3	79.1	2.4	23.7	9.5	7.1	201.2
6–8	1996	9 ± 0.5	16.6	18	76	7	27.3	7.7	3.3	0.06	11.3	31.3	1.4	1.2	134.4	37.0	0.265	1.2	40.2	78.9	2.4	23.8	9.8	7.1	196.8
8–10	1990	n.d.	16.2	18	75	7	27.0	7.9	3.2	0.08	10.6	32.6	1.5	1.1	139.0	38.7	0.290	1.2	42.6	82.6	2.5	24.6	9.7	7.6	209.0
10–12	1984	n.d.	17.3	18	75	7	26.9	8.0	3.0	0.07	10.8	35.8	1.6	1.1	144.5	40.3	0.310	1.2	42.0	86.5	2.9	26.7	10.3	7.6	217.8
12–14	1978	9 ± 0.4	16.9	19	74	7	26.6	8.2	2.7	0.07	10.5	35.8	1.3	1.1	133.3	48.3	0.420	1.2	43.4	83.8	3.0	45.3	10.4	8.0	199.2
14–16	1971	11 ± 0.6	16.7	16	76	7	26.5	8.0	3.0	0.07	10.1	35.5	1.6	1.2	143.4	43.0	0.345	1.2	44.4	85.2	2.9	35.9	10.1	7.7	212.5
16–18	1964	12 ± 0.6	17.3	19	74	8	26.5	8.0	3.0	0.07	10.6	35.3	1.6	1.1	139.3	43.7	0.365	1.3	42.7	83.2	2.7	32.8	10.4	7.8	207.9
18–20	1958	9 ± 0.4	18.1	21	72	7	26.5	8.0	2.9	0.06	10.6	37.3	1.7	1.1	142.6	46.1	0.395	1.2	41.7	85.3	2.8	35.1	10.5	8.0	210.4
20–22	1952	10 ± 0.5	17.3	18	74	8	26.4	8.0	2.9	0.07	11.4	40.1	1.7	1.1	150.3	47.8	0.380	1.3	44.5	88.5	3.1	37.9	11.2	8.5	219.3
22–24	1946	n.d.	17.1	19	73	8	26.7	8.2	2.9	0.06	11.4	40.5	1.5	1.2	140.1	47.0	0.475	1.2	44.6	84.0	3.0	41.2	10.8	8.1	207.8
24–26	1940	5 ± 0.3	19.6	24	68	8	26.8	8.0	2.9	0.07	10.3	36.5	1.7	1.2	149.7	41.9	0.330	1.2	45.1	88.8	2.8	29.9	10.3	7.9	213.4
26–28	1933	n.d.	18.7	24	68	8	26.7	8.3	2.7	0.05	11.3	40.4	1.2	0.9	127.0	47.4	0.410	1.1	43.7	80.9	2.9	46.8	10.4	7.8	184.0
28–30	1931	n.d.	15.1	18	74	9	26.7	8.4	2.6	0.06	10.5	38.5	1.2	0.8	124.2	46.3	0.400	1.0	42.3	78.1	2.8	46.5	10.1	7.5	171.5
30–32	1928	1 ± 0.3	15.6	17	75	9	26.7	8.4	2.4	0.04	10.9	38.4	1.1	0.8	128.3	45.3	0.395	1.1	42.3	79.5	2.9	49.6	10.0	7.5	166.1
32–34	1925	n.d.	17.4	21	71	8	26.4	8.6	2.3	0.05	9.8	39.4	1.1	0.7	129.2	44.3	0.405	1.1	41.8	80.6	3.0	53.7	9.9	7.6	166.5
34–36	1923	n.d.	14.1	16	75	9	26.4	8.5	2.2	0.05	10.5	39.4	1.1	0.9	135.8	43.1	0.385	1.1	43.7	81.5	2.9	53.9	10.2	7.1	164.1
36–38	1920	<d.l. ± 0.5	14.2	15	76	9	26.6	8.6	2.0	0.05	11.2	37.3	1.1	0.7	131.2	39.7	0.370	1.0	42.5	79.1	2.8	53.2	10.1	6.7	155.1
38–40	1917	<d.l. ± 0.5	14.6	18	73	9	26.6	8.7	1.9	0.05	10.8	37.6	1.0	0.8	135.8	39.6	0.380	1.0	43.2	79.4	2.9	49.6	10.4	6.7	151.4
40–42	1914	n.d.	14.4	16	74	9	26.5	8.7	1.8	0.05	10.7	36.4	1.0	0.8	132.2	37.2	0.350	0.9	42.7	75.9	2.6	41.9	10.5	6.6	143.5
42–44	1911	<d.l. ± 0.4	15.3	17	73	9	26.6	8.7	1.7	0.05	10.9	36.0	1.0	0.7	133.2	36.0	0.350	0.9	41.0	79.4	2.6	38.7	10.3	6.5	141.2
44–46	1908		14.6	16	74	10	26.6	8.6	1.6	0.02	11.8	37.0	1.0	0.9	130.7	35.8	0.340	1.0	43.9	76.1	2.6	32.3	10.7	7.0	137.7
46–48	1905		14.9	16	74	10	26.6	8.7	1.6	0.05	11.6	36.6	1.0	0.8	123.7	34.7	0.325	0.9	43.1	74.2	2.3	26.0	10.3	6.9	136.4
48–50	1902		19.3	23	68	9	27.2	8.6	1.1	0.03	13.0	32.7	0.9	0.7	105.8	27.8	0.255	0.9	40.8	63.8	2.0	14.4	10.7	6.3	121.3
50–52	1899		16.6	20	71	9	26.4	8.8	1.6	0.04	10.3	34.4	0.9	0.7	120.0	33.2	0.350	1.0	43.0	112.9	2.2	21.4	10.2	6.6	132.3
52–54	1896		18.0	20	71	9	26.6	8.7	1.6	0.04	11.9	36.3	0.9	0.7	113.3	31.9	0.395	1.0	41.9	66.4	2.2	19.4	10.4	6.5	128.6
54–56	1893		20.4	20	71	8	26.6	8.7	1.5	0.03	11.1	35.8	0.9	0.7	110.5	30.8	0.385	1.0	42.0	65.1	2.8	18.4	10.4	6.5	128.8
56–58	1891		21.5	25	67	8	26.5	8.7	1.6	0.03	10.8	34.3	0.9	0.6	105.7	30.1	0.300	0.9	41.7	63.2	2.1	16.1	10.4	6.6	126.7
58–60	1888		18.3	21	70	9	27.1	8.7	1.3	0.03	11.5	33.0	0.9	0.8	107.8	28.9	0.220	0.9	41.9	62.0	1.9	14.3	10.5	6.4	128.1
60–62	1885		14.8	18	72	10	26.5	8.7	1.6	0.04	12.5	34.9	0.9	0.7	120.9	33.0	0.315	1.0	42.7	182.4	2.3	25.7	10.6	6.9	133.1
62–64	1882		18.1	20	71	9	27.2	8.7	1.1	0.02	11.6	33.4	0.9	0.7	105.9	27.5	0.275	0.9	41.0	60.6	1.9	13.9	10.3	6.5	123.6
64–66	1879		18.7	22	69	9	27.7	8.7	0.9	0.04	12.2	31.2	0.9	0.5	103.3	26.6	0.175	0.9	41.1	57.6	1.8	12.7	10.2	6.2	123.5
66–68	1876		21.1	22	70	8	27.9	8.6	0.9	0.05	13.4	30.2	0.9	0.6	105.6	25.9	0.190	0.9	41.8	57.4	1.8	12.4	10.5	6.0	120.3
68–70	1873		19.0	22	69	9	27.7	8.7	0.9	0.05	11.4	30.5	0.8	0.6	101.1	27.4	0.180	0.9	43.2	55.8	1.8	11.8	10.0	6.0	122.0
70–72	1870		18.1	20	71	9	27.5	8.6	0.9	0.05	12.6	29.7	0.9	0.7	100.4	26.5	0.180	0.9	43.0	55.8	1.8	11.3	10.0	6.3	123.0
72–74	1867		18.5	20	71	9	27.7	8.6	0.8	0.06	12.3	30.2	0.8	0.6	100.8	27.3	0.145	0.8	43.3	55.7	1.8	12.2	10.3	5.9	126.1
74–76	1864		18.0	19	72	9	27.7	8.8	0.8	0.06	11.1	31.8	0.9	0.6	100.0	25.1	0.088	0.8	38.4	54.2	1.8	10.8	9.7	6.9	122.0
76–78	1861		15.8	18	72	10	27.5	8.8	0.7	0.06	11.6	32.0	0.9	0.6	100.6	25.5	0.079	0.8	41.4	53.9	1.9	10.6	9.9	5.7	121.3
78–80	1858		17.8	18	73	9	27.8	8.6	0.7	0.05	11.1	29.8	0.8	0.6	95.7	23.4	0.064	0.8	38.4	51.7	1.8	10.5	10.3	5.9	115.8
80–82	1855		16.4	15	75	9	27.9	8.7	0.8	0.05	11.5	29.9	0.9	0.6	98.9	24.1	0.077	0.8	39.1	53.4	1.8	10.6	10.3	5.9	116.9
82–84	1852		16.0	14	77	10	28.1	8.6	0.7	0.06	11.7	30.7	0.9	0.6	99.4	23.4	0.064	0.9	38.8	52.3	1.7	9.8	9.9	6.0	120.8
84–86	1849		16.7	15	75	9	27.8	8.7	0.7	0.04	12.1	29.0	0.9	0.5	99.2	22.9	0.073	0.9	38.5	51.4	2.0	10.2	9.9	5.7	114.3
86–88	1846		17.2	17	73	10	28.5	8.5	0.6	0.05	11.1	28.5	0.8	0.5	92.2	20.6	0.058	0.7	36.2	49.3	1.7	9.4	9.5	5.9	108.7
88–90	1844		14.6	14	76	10	27.9	8.8	0.7	0.06	11.2	29.8	0.8	0.6	96.4	22.9	0.058	0.7	38.4	51.8	1.9	10.0	9.8	5.9	118.9
90–92	1841		12.2	11	78	11	28.3	8.7	0.6	0.05	10.6	29.7	0.8	0.5	92.7	20.7	0.054	0.7	36.2	49.2	1.7	9.2	9.4	6.0	110.8

92–94	1838	13.6	14	76	11	28.2	8.6	0.6	0.05	11.0	28.3	0.8	0.5	93.6	20.4	0.052	0.7	36.3	48.8	1.7	9.3	9.7	6.0	108.8
94–96	1836	16.7	17	73	10	28.4	8.7	0.5	0.06	11.7	29.4	0.8	0.5	95.3	21.1	0.045	0.8	37.3	49.8	1.8	8.7	10.4	5.9	110.3
96–98	1833	14.3	14	75	10	28.5	8.5	0.5	0.05	11.1	25.1	0.8	0.5	90.2	19.3	0.041	0.7	35.0	44.9	1.6	8.1	9.2	5.2	100.3
98–100	1831	17.7	15	77	9	28.3	8.5	0.5	0.06	11.3	26.4	0.8	0.6	91.3	20.3	0.041	0.8	35.2	46.3	1.6	8.2	10.1	5.7	103.1
100–102	1828	16.1	16	75	9	28.5	8.5	0.5	0.06	12.1	26.4	0.8	0.6	94.2	20.5	0.044	0.8	34.3	47.2	1.6	8.5	9.8	5.8	107.1
102–104	1826	17.1	15	76	9	27.1	9.0	0.6	0.06	9.6	28.1	0.9	0.4	99.3	24.2	0.053	0.9	39.1	49.3	1.7	8.8	9.5	5.6	120.4
104–106	1824	14.0	10	80	10	26.7	9.2	0.7	0.07	9.3	27.7	0.9	0.5	98.5	25.8	0.056	0.9	39.2	51.4	1.8	9.0	9.1	5.6	124.7
106–108	1821	13.3	12	77	11	27.2	8.9	0.6	0.06	9.7	32.5	0.9	0.4	97.8	24.8	0.045	0.9	37.8	53.2	1.8	11.1	9.3	6.3	125.2
108–110	1819	15.9	15	76	10	26.4	9.1	0.6	0.07	9.2	33.0	0.9	0.4	99.4	26.4	0.046	1.0	41.0	52.2	1.9	9.2	9.1	5.8	126.6
110–112	1816	12.6	10	79	11	26.0	9.2	0.7	0.07	8.7	31.2	0.9	0.5	97.8	27.1	0.049	0.9	42.7	51.7	1.8	9.0	9.3	5.8	127.6
112–114	1814	9.9	10	77	13	27.1	8.8	0.6	0.06	10.6	30.0	0.9	0.4	94.4	24.3	0.046	0.9	39.4	52.0	1.8	8.9	9.7	5.8	120.1
114–116	1812	17.3	20	70	10	27.0	8.9	0.6	0.05	10.5	30.3	0.9	0.5	94.7	23.9	0.058	0.8	40.9	53.0	2.0	8.7	9.7	5.8	120.3
116–118	1809	13.4	14	75	11	27.1	8.9	0.7	0.05	10.7	38.0	0.9	0.4	103.7	25.5	0.054	0.9	38.5	57.7	2.4	9.1	9.7	6.1	127.4
118–120	1807	15.9	17	73	10	28.1	8.4	0.5	0.05	13.4	31.8	0.8	0.5	96.1	22.0	0.047	0.8	34.3	55.1	2.0	8.6	9.8	6.1	111.7
120–122	1804	18.1	18	72	10	28.4	8.3	0.5	0.02	13.1	30.8	0.8	0.4	96.2	21.1	0.046	0.8	35.2	53.4	1.8	8.7	9.9	6.0	105.4
122–124	1802	36.4	36	57	7	28.1	8.2	0.5	0.02	14.6	33.3	0.8	0.5	95.9	22.0	0.041	0.8	36.5	53.4	1.9	8.4	10.7	6.0	106.6
124–126	1799	28.9	29	64	7	27.8	8.6	0.5	0.02	14.5	30.4	0.8	0.5	98.7	22.6	0.042	0.8	37.7	52.3	1.7	8.6	10.6	6.0	111.6
126–128	1797	16.1	19	72	9	27.0	9.0	0.7	0.02	11.4	27.1	0.9	0.4	101.3	25.8	0.049	0.9	42.5	56.2	1.8	8.9	9.6	5.8	125.0
128–130	1794	24.2	33	58	9	27.1	8.8	0.7	0.02	11.8	28.6	0.9	0.4	99.2	25.0	0.053	0.8	39.0	58.3	1.9	9.0	10.1	5.9	121.2
130–132	1792	26.4	29	63	8	28.2	8.4	0.6	0.02	15.3	27.5	0.8	0.7	99.0	21.5	0.043	0.8	38.9	56.6	1.7	11.1	11.3	6.3	110.9
132–134	1790	37.9	36	57	7	29.2	8.0	0.5	0.02	20.9	25.0	0.8	0.7	96.7	19.5	0.037	0.9	37.0	55.6	1.7	8.7	13.5	6.0	103.8
134–136	1787	33.8	32	62	6	29.4	7.9	0.5	0.03	24.9	21.0	0.8	0.8	94.7	19.7	0.032	0.7	33.5	52.1	1.6	8.1	16.9	5.7	99.9
136–138	1785	25.4	28	64	8	27.1	8.5	0.6	0.02	14.1	30.3	0.9	0.6	103.1	24.8	0.041	1.0	42.1	63.0	1.7	8.1	10.6	5.6	117.2
138–140	1783	22.2	24	67	9	27.8	8.4	0.6	0.03	15.0	28.5	0.9	0.6	101.7	23.6	0.041	0.8	40.1	68.7	2.0	8.6	11.4	6.0	116.1
140–142	1780	24.4	26	66	8	27.5	8.4	0.6	0.03	12.7	31.6	0.8	0.5	98.4	22.6	0.038	0.9	39.4	53.9	2.1	8.0	10.8	5.5	110.1
142–144	1778	19.0	23	67	10	27.1	8.9	0.6	0.02	11.2	28.4	0.9	0.5	98.2	24.1	0.042	0.9	41.2	49.4	2.0	8.2	9.1	5.3	115.6
144–146		18.3	26	64	10	27.1	8.9	0.7	0.02	11.1	27.5	0.9	0.5	97.5	24.8	0.045	0.8	41.9	51.9	2.2	8.8	8.8	5.5	117.3
146–148		22.2	32	59	10	26.9	8.8	0.7	0.02	10.8	34.0	0.9	0.5	97.4	25.5	0.044	0.8	38.8	52.5	2.2	10.2	9.2	5.7	118.0
148–150		42.4	41	53	6	29.6	7.9	0.5	0.01	20.7	18.5	0.7	0.7	99.6	19.1	0.028	0.6	34.0	50.7	1.7	8.5	12.6	5.5	101.4
150–152		65.7	52	44	4	30.1	7.8	0.4	0.01	22.0	20.8	0.7	0.7	95.6	18.1	0.093	0.7	33.7	50.4	1.6	7.7	12.5	5.2	93.3
152–154		52.4	45	49	6	29.8	7.6	0.4	0.01	18.7	28.6	0.7	0.6	90.4	17.4	0.034	0.7	34.4	51.1	1.7	7.3	11.6	5.5	93.0
154–156		96.0	67	30	3	30.3	7.7	0.5	0.02	22.3	17.3	0.7	0.8	91.2	17.9	0.024	0.6	30.4	56.6	1.7	8.0	13.6	5.9	93.0
156–158		67.9	53	43	4	30.7	7.4	0.4	0.02	27.5	24.5	0.7	1.0	91.4	15.9	0.018	0.6	26.9	47.5	1.5	7.6	15.3	5.9	83.1
158–160		66.8	52	43	4	30.4	7.6	0.4	0.01	23.3	36.9	0.7	0.8	92.6	16.5	0.027	0.8	31.2	47.1	1.5	7.8	13.1	5.5	87.6
160–162		141.0	78	20	2	31.0	7.6	0.4	0.02	20.8	27.3	0.7	0.7	92.2	17.5	0.019	0.7	30.6	48.2	1.9	8.5	12.1	5.6	93.9
162–164		154.0	82	16	1	31.3	7.4	0.4	0.02	31.8	23.7	0.7	1.1	91.8	17.3	0.016	<	29.3	48.1	1.6	7.4	16.8	5.6	96.2
164–166		86.4	60	37	3	30.0	7.5	0.4	0.01	18.1	27.4	0.6	0.6	89.6	19.2	0.021	0.7	33.0	48.7	1.5	6.8	11.3	5.2	88.7
166–168		112.0	70	28	2	30.8	7.3	0.4	0.01	26.7	31.5	0.7	0.8	88.3	14.3	0.022	0.7	30.8	46.4	1.5	7.0	15.6	5.0	81.4
168–170		146.0	74	24	2	30.5	7.6	0.5	0.01	24.2	23.0	0.7	0.7	88.6	15.0	0.023	0.6	32.3	48.7	1.5	6.6	14.8	4.7	84.4
170–172		164.8	85	14	1	30.3	7.6	0.5	0.01	24.4	19.5	0.7	0.7	92.4	16.2	0.018	0.6	33.3	51.2	1.6	6.8	15.4	4.9	88.7
172–174		117.9	71	26	2	30.8	7.4	0.4	0.01	26.8	21.8	0.7	0.8	91.6	14.1	0.018	0.6	31.1	49.5	1.5	6.9	16.0	5.1	83.8
174–176		128.0	74	24	2	29.9	7.8	0.5	0.01	27.0	19.6	0.8	0.8	97.9	19.6	0.026	0.7	34.3	56.2	1.8	8.7	16.4	5.5	98.4
176–178		111.7	71	26	3	30.4	7.4	0.4	0.01	37.3	20.2	0.7	1.0	99.0	14.8	0.026	0.7	33.2	50.5	1.7	8.3	22.1	5.1	84.3
178–180		30.4	31	62	7	28.5	8.3	0.7	0.02	14.3	24.9	0.8	0.5	104.2	19.9	0.038	0.8	36.2	57.8	2.0	7.9	11.2	5.5	110.6
180–182		100.2	65	32	3	29.8	7.8	0.7	0.01	33.4	18.4	0.8	1.0	109.8	17.9	0.030	0.7	32.6	59.3	1.8	8.6	20.2	5.6	99.0
182–184		16.9	18	72	10	27.0	8.8	0.8	0.02	13.7	25.5	0.9	0.6	102.6	22.9	0.062	0.9	40.4	55.3	1.8	9.0	11.1	5.3	117.6
184–186		27.9	36	57	8	25.5	9.1	0.8	0.02	8.7	46.2	0.9	0.4	109.9	26.9	0.068	1.1	48.5	55.9	1.8	9.4	9.0	5.2	137.0
186–188		22.8	30	62	8	27.9	8.7	0.9	0.02	15.6	24.3	0.9	0.5	105.7	23.5	0.048	0.8	39.4	59.8	1.8	9.8	12.0	5.9	117.7
188–190		194.5	69	28	3	29.5	8.3	0.7	0.02	15.5	16.2	0.8	0.6	101.4	20.1	0.041	0.7	33.7	58.3	1.7	8.4	11.6	5.5	103.3
190–192		397.4	96	4	1	30.7	7.6	0.6	< d.l.	25.4	26.0	0.6	0.7	94.3	15.3	0.034	1.0	32.8	47.0	1.6	17.2	15.7	4.6	81.5
192–194		508.5	97	2	0																			
194–196		467.9	98	2	0																			
196–198		435.3	98	2	0																			
198–200		402.4	95	4	0																			
200–202		599.4	97	3	0																			

Table 2
Selected major and trace element concentrations in the <63 μm sediments according to depth, Cs activity, median grain size (D_{50}) and percentages of sands (63 μm–2 mm), silts (2–63 μm) and clays (<2 μm) in the bulk sediment layers of the paleochannel core (UWC). n.d. = not determined; <d.l. = below the detection limit.

Depth (cm)	Age (y)	^{137}Cs (Bq/kg)		D_{50} (μm)	Sand (>63 μm) (%)	Silt (2–63 μm) (%)	Clay (<2 μm) (%)	Si (%)	Al (%)	TOC (%)	S tot. (%)	Hf (ppm)	As (ppm)	Bi (ppm)	Cd (ppm)	Cr (ppm)	Cu (ppm)	Hg (ppm)	Mo (ppm)	Ni (ppm)	Pb (ppm)	Sb (ppm)	Sn (ppm)	U (ppm)	W (ppm)	Zn (ppm)
0–2	2012	6 + −	0.7	30.1	27	71	2	29.2	7.0	2.9	0.10	11.8	27.9	0.9	1.0	96.2	26.5	0.110	0.9	32.7	61.5	1.8	10.8	7.4	6.0	158.8
2–4	2009	n.d.	n.d.	31.2	28	70	2	28.5	7.1	3.1	0.09	11.0	29.1	1.0	1.0	100.8	32.5	0.130	0.8	35.2	68.4	1.8	13.4	7.9	6.7	174.0
4–6	2007	n.d.	n.d.	28.6	26	71	2	29.0	7.1	2.8	0.10	11.4	25.1	1.0	1.0	101.0	30.6	0.115	0.8	35.4	66.2	1.8	11.7	7.6	6.4	166.4
6–8	2005	n.d.	n.d.	31.2	29	69	2	30.0	7.0	2.5	0.09	13.1	24.4	0.9	1.0	100.7	29.2	0.120	0.7	34.4	65.2	1.8	11.4	8.3	6.1	160.0
8–10	2002	n.d.	n.d.	27.8	26	71	3	30.5	6.9	2.2	0.08	15.2	24.0	0.9	0.8	99.2	29.0	0.150	0.7	34.9	66.6	1.8	11.9	8.7	6.0	154.8
10–12	1999	7 + −	0.7	44.9	41	57	2	30.6	6.9	2.1	0.08	15.0	23.7	0.9	0.8	99.2	28.1	0.105	0.8	34.3	66.2	1.7	12.6	8.7	6.3	149.4
12–14	1997	5 + −	0.5	45.5	41	57	2	30.4	7.0	2.2	0.09	15.2	23.2	1.0	0.9	103.2	27.9	0.110	0.8	35.1	66.7	1.9	13.3	8.5	6.4	161.0
14–16	1994	7 + −	0.8	39.2	37	60	2	30.3	7.1	2.2	0.10	15.7	24.4	1.0	1.0	118.5	29.8	0.280	0.9	39.6	78.9	1.9	13.5	9.6	6.5	169.7
16–18	1991	n.d.	n.d.	39.5	37	60	2	30.0	7.1	2.2	0.11	14.7	26.4	1.0	1.1	162.0	33.6	0.180	1.1	48.5	104.2	2.0	14.8	9.1	6.8	194.1
18–20	1987	9 + −	0.5	36.8	36	62	2	30.2	7.1	2.2	0.10	16.3	25.5	1.2	1.2	166.8	30.2	0.200	1.1	49.5	112.2	1.9	14.8	10.1	6.5	196.4
20–22	1984	9 + −	0.7	41.8	39	58	2	30.2	7.2	2.2	0.10	15.9	25.4	1.1	1.1	177.1	36.2	0.220	1.1	51.9	143.6	2.2	15.7	9.6	6.7	211.7
22–24	1981	n.d.	n.d.	42.1	40	58	2	30.0	7.2	2.3	0.11	15.0	28.4	1.5	1.3	208.8	40.3	0.255	1.1	57.3	199.5	2.2	16.9	9.1	6.8	237.9
24–26	1978	12 + −	0.8	36.8	35	62	2	30.7	7.1	2.2	0.11	16.6	26.7	1.4	1.3	202.4	35.9	0.185	1.1	56.7	252.9	2.1	15.0	9.3	6.7	229.0
26–28	1974	13 + −	0.4	41.2	39	58	2	30.8	7.2	2.1	0.11	14.9	26.8	1.6	1.2	181.0	35.0	0.185	1.1	51.6	255.4	2.1	17.3	9.0	7.7	225.2
28–30	1969	14 + −	0.5	40.1	38	59	3	30.8	7.2	2.0	0.12	15.0	24.8	1.5	1.2	160.9	33.5	0.195	1.0	48.8	201.8	2.1	14.8	9.0	6.7	230.6
30–32	1964	17 + −	0.8	43.1	41	57	3	30.6	7.2	2.0	0.11	16.1	25.4	2.3	1.4	156.3	33.9	0.170	1.1	47.3	193.7	2.2	15.4	10.0	7.2	239.4
32–34	1960	12 + −	0.6	41.6	40	58	2	29.9	7.3	2.2	0.14	17.1	28.9	1.7	1.8	178.0	42.2	0.330	1.2	58.1	170.0	2.3	16.6	11.1	7.4	359.3
34–36	1957	12 + −	0.6	44.3	41	57	2	30.0	7.4	2.7	0.20	16.4	33.6	2.7	2.4	222.0	57.4	0.255	1.4	76.7	133.9	3.0	21.2	10.6	7.7	536.0
36–38	1955	9 + −	0.7	32.6	31	66	3	28.4	7.6	3.7	0.38	12.9	39.4	3.4	3.0	240.0	88.9	0.575	2.0	89.5	107.2	4.1	24.7	15.4	8.8	614.4
38–40	1952	n.d.	n.d.	39.7	39	59	2	27.6	7.7	4.6	0.47	12.0	41.7	2.9	2.8	244.2	110.4	0.720	2.4	92.8	106.2	4.8	29.6	19.2	8.8	598.9
40–42	1948	< d.l.	1.0	69.9	52	46	2	27.4	7.8	4.9	0.45	11.7	41.1	2.8	2.4	217.5	114.2	0.895	2.3	83.0	96.6	4.6	29.0	18.2	8.4	542.5
42–44	1944	n.d.	n.d.	36.4	37	60	3	28.0	7.8	4.1	0.35	16.0	33.4	1.3	1.4	129.0	95.4	0.570	1.5	51.2	84.9	3.7	38.1	12.2	7.2	292.3
44–46	1940	n.d.	n.d.	49.7	45	52	3	28.2	8.0	3.0	0.30	13.4	32.4	1.0	1.0	126.9	65.5	1.080	1.2	40.6	91.2	3.6	55.8	10.4	7.3	199.7
46–48	1936	< d.l.	0.6	31.1	32	64	3	28.2	8.0	2.6	0.18	13.7	27.6	1.0	0.9	126.1	52.4	0.410	0.9	39.3	87.0	2.9	60.7	10.4	6.7	179.5
48–50	1933	n.d.	n.d.	32.4	37	60	3	27.7	8.4	2.9	0.21	11.7	32.7	1.0	0.8	131.5	48.3	0.450	1.0	40.4	90.7	3.1	71.3	9.6	6.8	178.7
50–52	1931	n.d.	n.d.	17.7	21	74	5	26.2	9.0	2.3	0.15	8.6	30.1	1.0	0.6	170.7	43.1	0.420	0.9	45.5	91.7	3.0	58.9	8.3	5.8	162.3
52–54	1930	< d.l.	0.7	17.5	19	77	5	26.4	8.8	2.7	0.13	8.5	31.7	1.0	0.7	180.5	44.8	0.480	0.9	42.7	109.4	3.6	77.2	8.2	5.6	160.3
54–56	1928	n.d.	n.d.	13.7	8	86	6	26.1	9.0	2.6	0.11	7.5	29.3	1.1	0.6	171.5	68.8	0.505	1.0	41.2	114.0	3.9	81.9	8.5	6.1	181.1
56–58	1927	n.d.	n.d.	18.0	19	76	5	27.2	8.5	2.4	0.10	8.8	29.2	1.1	0.7	177.0	37.6	0.470	1.0	37.9	112.2	3.4	64.9	8.6	6.5	156.6
58–60	1925	< d.l.	0.7	16.7	15	79	5	27.2	8.7	2.0	0.07	8.7	23.3	0.9	0.5	158.7	33.9	0.395	0.8	40.8	84.2	2.5	29.0	8.7	6.0	140.1
60–62	1922			19.6	20	75	5	27.2	8.6	2.2	0.08	9.5	23.4	1.0	0.5	157.3	34.7	0.465	0.9	40.5	80.5	2.4	26.6	9.0	5.7	141.5
62–64	1920			27.8	31	65	4	28.1	8.3	2.1	0.07	11.7	22.9	0.9	0.6	157.8	33.3	0.435	0.8	36.9	79.3	2.7	22.2	9.4	5.9	131.7
64–66	1918			19.0	21	74	5	28.0	8.3	2.2	0.09	10.5	27.0	0.9	0.6	174.5	36.5	0.450	0.8	38.0	78.1	2.6	23.3	9.4	6.3	145.1
66–68	1917			21.1	23	73	4	27.8	8.3	2.3	0.09	10.0	29.4	1.0	0.6	164.6	37.0	0.405	0.7	39.0	75.1	2.3	22.1	8.8	6.0	142.5
68–70	1915			20.1	21	75	4	27.8	8.3	2.4	0.09	10.3	29.4	0.9	0.6	156.6	35.8	0.410	0.8	39.5	73.5	2.3	20.8	9.0	5.9	139.9
70–72	1913			20.0	21	75	4	27.4	8.4	2.3	0.10	9.8	29.7	0.9	0.6	152.2	35.7	0.385	0.8	39.4	73.5	2.3	20.9	9.1	6.1	140.9

72–74	1910	20.3	20	76	4	26.7	8.6	2.3	0.11	9.4	28.6	0.9	0.6	120.2	32.0	0.315	1.1	40.7	66.1	2.0	15.1	8.9	5.7	136.8
74–76	1907	34.5	40	56	4	27.5	8.5	2.0	0.08	10.4	26.8	0.9	0.6	96.6	29.3	0.275	0.9	37.5	64.6	2.0	12.7	9.5	5.8	135.5
76–78	1907	25.0	30	66	4	27.4	8.5	2.1	0.08	10.4	25.2	0.8	0.6	97.7	26.8	0.250	0.8	39.1	61.5	1.7	11.8	9.2	5.8	127.8
78–80	1907	24.0	29	66	5	27.3	8.4	2.1	0.08	10.7	24.1	0.8	0.5	94.7	25.3	0.225	0.7	37.9	58.3	1.7	10.9	8.9	6.3	121.6
80–82	1903	14.9	14	79	7	27.4	8.6	1.8	0.06	9.7	23.4	0.9	0.5	96.9	26.0	0.235	0.7	39.4	55.6	1.6	10.7	8.4	6.3	126.7
82–84	1899	20.7	22	72	5	27.4	8.5	1.5	0.07	11.4	25.7	0.9	0.5	92.2	25.4	0.290	0.7	36.7	61.4	1.8	10.9	9.2	7.4	126.5
84–86	1895	18.9	20	74	6	26.7	8.2	1.4	0.07	9.8	27.6	0.9	0.5	91.6	25.3	0.485	0.8	35.5	64.6	1.9	11.9	8.4	6.8	125.7
86–88	1891	20.4	20	75	5	27.9	8.2	1.3	0.06	10.4	25.7	0.8	0.5	89.5	24.1	0.555	0.6	35.7	63.1	1.6	10.5	8.4	6.2	120.9
88–90	1888	14.1	13	80	7	27.2	8.5	1.4	0.08	9.2	28.8	0.9	0.6	92.9	25.3	0.605	0.7	37.5	69.3	1.8	11.5	8.3	6.4	130.8
90–92	1885	22.4	24	72	5	28.6	8.5	1.2	0.06	12.4	34.5	1.0	0.7	98.2	24.3	0.425	0.8	37.1	80.3	2.1	13.9	9.2	7.8	120.0
92–94	1880	23.4	23	72	5	28.2	8.5	1.0	0.05	11.2	29.7	0.9	0.6	94.1	18.8	0.215	0.8	36.2	66.6	2.0	12.1	8.9	7.0	108.2
94–96	1875	18.2	18	75	7	28.1	8.7	1.0	0.05	10.9	30.1	1.0	0.6	98.6	23.3	0.071	0.8	39.0	63.9	2.2	13.2	9.1	7.2	112.7
96–98	1871	16.5	18	76	6	27.4	8.8	1.2	0.06	9.9	31.5	1.0	0.6	95.2	23.5	0.100	0.9	37.1	63.7	2.2	12.1	8.6	6.8	114.6
98–100	1866	30.6	33	63	4	28.0	8.6	1.2	0.05	12.1	29.7	1.0	0.7	91.2	22.4	0.063	0.8	35.4	60.8	2.3	11.7	9.2	6.5	107.8
100–102	1861	21.4	21	74	5	28.0	8.7	1.1	0.05	12.4	30.2	1.0	0.6	93.3	23.6	0.066	0.9	36.2	60.2	2.2	11.4	9.6	6.5	109.2
102–104	1856	25.9	33	62	5	27.3	8.9	1.1	0.08	9.9	31.4	1.1	0.6	91.3	23.9	0.060	0.9	37.0	60.2	1.9	10.8	8.5	6.6	113.5
104–106	1854	15.7	14	80	7	28.3	8.8	1.0	0.07	9.6	29.6	1.1	0.5	91.3	22.6	0.058	0.9	35.4	61.7	2.0	11.8	8.6	7.0	109.9
106–108	1853	18.0	17	77	6	28.1	8.7	1.1	0.06	9.7	28.4	1.0	0.6	89.0	22.5	0.063	0.8	35.5	59.4	1.9	10.8	8.1	6.4	108.9
108–110	1851	15.5	13	80	7	28.2	8.7	1.0	0.06	10.7	28.9	1.0	0.6	88.7	21.8	0.051	0.8	35.4	58.0	1.7	10.8	8.5	6.2	107.7
110–112	1850	21.3	19	76	5	28.0	8.7	1.0	0.06	10.4	31.9	1.0	0.6	100.7	23.9	0.049	0.9	40.7	59.6	2.0	11.4	8.9	6.0	117.4
112–114	1848	17.7	15	79	6	28.4	8.5	1.0	0.04	10.9	29.4	0.9	0.6	91.1	21.5	0.045	0.9	38.1	55.9	1.8	10.5	8.5	6.1	106.2
114–116	1846	21.0	22	73	5	27.4	9.0	1.1	0.04	9.2	31.7	1.0	0.6	96.9	25.5	0.067	1.0	41.4	58.7	1.8	10.4	8.4	5.8	119.6
116–118	1846	24.2	30	65	6	29.1	8.4	0.9	0.05	10.8	29.7	0.9	0.5	88.6	19.6	0.036	0.8	33.0	56.7	1.9	9.9	9.1	6.3	100.2
118–120	1843	15.1	13	80	7	27.5	8.7	1.1	0.06	8.9	33.1	1.2	0.6	90.1	22.4	0.049	0.9	37.3	59.2	2.0	10.9	8.4	6.3	112.1
120–122	1840	14.9	15	78	7	27.8	8.7	1.1	0.06	9.2	35.4	1.1	0.6	94.2	22.2	0.047	0.9	36.1	62.3	2.4	11.3	8.6	7.3	116.1
122–124	1837	12.8	9	83	8	27.9	8.7	1.1	0.06	9.2	35.6	1.1	0.6	88.5	22.6	0.045	0.9	34.9	63.3	2.5	10.9	8.8	7.5	117.6
124–126	1833	16.2	15	79	7	27.4	8.6	1.0	0.05	9.4	33.0	1.1	0.6	91.2	22.0	0.043	0.8	35.6	60.4	2.2	10.5	8.6	6.9	110.7
126–128	1830	14.7	13	80	7	27.0	8.8	1.0	0.06	8.5	32.7	1.0	0.6	92.1	25.4	0.051	0.8	36.4	61.4	2.1	10.9	8.6	7.1	126.4
128–130	1827	13.2	8	86	7	26.9	8.8	1.3	0.06	8.7	32.6	1.0	0.6	89.1	23.5	0.046	0.9	37.0	58.5	2.0	10.6	8.5	6.8	116.4
130–132	1824	13.1	13	80	7	26.6	9.2	1.1	0.07	7.7	37.1	1.1	0.5	97.0	26.0	0.050	1.0	40.5	60.1	2.0	11.0	7.9	6.9	127.3
132–134	1821	11.1	6	85	8	26.9	9.2	1.3	0.07	7.5	35.7	1.1	0.6	91.7	24.8	0.055	0.9	37.8	61.2	2.0	11.1	7.9	7.4	124.6
134–136	1819	10.1	4	87	9	26.6	9.3	1.3	0.05	7.0	36.3	1.1	0.6	92.7	25.0	0.049	0.9	38.2	61.4	2.1	11.7	7.8	7.4	127.0
136–138	1816	12.9	12	81	7	26.4	9.4	1.3	0.07	7.1	33.4	1.0	0.4	102.6	27.3	0.051	1.0	44.1	54.2	2.0	10.1	8.4	6.5	138.7
138–140	1813	7.8	6	82	12	26.7	9.4	1.2	0.07	6.8	36.5	1.0	0.5	96.0	26.1	0.044	1.0	37.5	58.4	2.2	10.2	8.4	6.7	132.4
140–142	1810	12.7	9	85	7	27.3	8.8	1.3	0.07	8.1	31.5	0.9	0.5	94.2	23.3	0.053	0.8	37.4	55.0	1.9	9.2	8.2	6.0	127.5
142–144	1807	18.1	15	79	6	28.0	8.6	1.1	0.06	10.4	28.9	0.8	0.5	94.7	23.1	0.046	0.8	36.4	54.7	2.0	9.8	9.0	6.0	124.9
144–146	1804	15.6	13	80	7	27.6	8.7	1.1	0.06	9.5	28.3	0.8	0.5	95.6	23.3	0.047	0.8	36.8	56.4	2.1	9.6	9.2	6.2	129.7
146–148	1800	16.1	17	77	6	28.4	8.6	1.0	0.05	10.7	26.7	0.8	0.5	93.4	22.0	0.042	0.7	36.2	52.4	1.8	8.6	9.2	5.8	118.6
148–150	1797	13.8	10	82	7	27.3	8.8	1.0	0.05	9.7	27.0	0.8	0.5	103.2	23.8	0.047	0.8	41.5	52.4	1.6	8.2	8.7	5.2	124.6
150–152	1794	13.0	12	80	8	27.8	8.7	1.0	0.06	10.6	26.7	0.8	0.5	99.0	22.4	0.042	0.8	39.4	52.7	1.6	8.0	9.0	5.3	119.6
152–154	1791	15.5	14	78	7	27.8	8.7	1.0	0.05	10.7	27.5	0.9	0.5	99.8	22.9	0.044	0.8	40.0	57.8	1.8	8.6	9.2	5.6	120.8
154–156	1787	17.6	17	77	7	27.9	8.7	0.9	0.02	11.2	26.5	0.8	0.4	101.8	22.5	0.039	0.8	39.3	51.4	1.8	8.1	9.1	5.3	117.1
156–158	1783	21.1	20	73	6	28.4	8.5	0.9	0.03	13.0	24.5	0.8	0.4	99.6	20.9	0.032	0.8	38.5	52.4	1.7	8.3	10.2	5.1	111.5
158–160	1778	29.7	30	66	5	29.4	8.1	0.8	0.03	18.3	23.2	0.7	0.5	98.2	18.2	0.026	0.7	35.8	50.9	1.7	8.1	12.8	5.5	105.1

extreme flood events, as shown by Dieras et al. (2013) in the Rhône River basin. However, preserving extreme flood deposits is limited in river banks (like RBC) because of strong erosion with these catastrophic discharges (Benedetti, 2003). Erosional control of river bank accretion is particularly strong for embanked rivers, as in the study area (Thompson and Croke, 2013; Fuller, 2008).

In the UWC, the preservation of flood sequences denotes a high level of archiving capacity and a nearly continuous record. In the RBC, their absence notes the importance of a topographic control on accretion and sediment preservation.

3.2. Time correlation and mass accumulation rate comparisons

3.2.1. Time correlation of sedimentary archives

In addition to archiving capacity and accretion continuity, the aggradation rate is an important factor influencing the resolution of temporal analyses. Spatial and temporal variability of aggradation rates across the floodplain can be highlighted by comparing the two cores. The first step of this analysis consists on a time correlation using specific temporal anchoring markers.

First, based on ^{137}Cs vertical profiles, specific time markers can be defined. In these cores, the ^{137}Cs is not detectable less than 36 cm deep in the RBC and 40 cm deep in the UWC (Tables 1 and 2). Sediments archived below these depths were settled before 1950, which was the date of the first important Nuclear Weapon Test (NWT). Gamma activities, measured between the surface and 36 or 40 cm deep, have large peaks at 16–18 cm deep for RBC and at 30–32 cm deep for the UWC (Tables 1 and 2). These sedimentary layers can be associated with the NWT maximum fallouts in 1964. The study area was barely impacted by the Chernobyl Nuclear Power Plant Disaster (C-NPPD) fallout of 1986 (De Cort et al., 1998). The measured ^{137}Cs patterns do not involve secondary peaks related to this event.

To refine the time correlation, additional relative time markers can be determined with sedimentary records associated with well dated hydrosedimentary events, such as flood events or climate and anthropogenic river forcing. The Decize Dam elevation of 1933 should influence sedimentation up to 50 cm deep for the UWC. In the upper unit of the RBC, only one sandy layer is recorded at 24–28 cm, likely related to the Decize Dam elevation, which should have triggered better preservation conditions. This hydrosedimentary event may be correlated to the three coarsest layers archived in the dam impacted unit of the UWC (48–50 cm, 44–46 cm and 40–42 cm; Fig. 2). The sedimentary transition dating is consistent with the ^{137}Cs absence under 40 cm (<1950) in the UWC. However, this time correlation holds for the RBC, where the ^{137}Cs vertical distribution does not conform to the common pattern described in the literature (^{137}Cs peak at 16–18 cm and some radionuclide was detected until 36 cm). In the pedogenetic context of the top 80 cm of the RBC, the ^{137}Cs vertical profile has to be interpreted cautiously because of roots and macrofauna bioturbation associated with solute transport. All of these mechanisms may be responsible for the downward migration of the radionuclide (Détriché et al., 2010; Matisoff et al., 2011). Additionally, the four flood sequences in the deepest unit of UWC at 114–118 cm, 102–104 cm, 98–100 cm, and 74–80 cm deep, can be dated to be 1846, 1856, 1866 and 1907, respectively, which are the four catastrophic floods events documented at the Decize gauging station.

3.2.2. Temporal and spatial variability of the mass accumulation rate

To compare the aggradation rhythm between the two cores, age-models can be set up between time markers. Age-models are built using mass accumulation rates (MARs), calculated between each dated level. The sandy sequence of the proximal floodplain aggradation, of the RBC, is considered contemporary at the end of the LIA (between 1760 and 1820). Detailed age models are only defined for the fine-grained sedimentation, *i.e.*, the whole UWC core and up to 144 cm for the RBC.

To refine the age-model, dates were calculated with respective MARs calculated between each date-bounded. For the UWC, a constant MAR of 1.3 kg·m^{-2}·year^{-1} can be calculated between the 2012 and the 1933 time marker, both bounding the upper unit. However, the MAR varies by 8% of this value by focusing on the 2012–1964 period or the 1964–1933 period (Fig. 3). The maximum error associated with these estimates is ±6 years. For the deepest unit of the UWC, a constant MAR of 2.3 kg·m^{-2}·year^{-1} is calculated between the 1933 and the 1846 time marker. More precisely, the MAR ranges between 1.7 and 4.4 kg·m^{-2}·year^{-1} between dated flood sequences (Fig. 3). The maximum time deviation corresponding to this variability reaches 11 years. There is no time marker below the 118 cm deep sedimentary level (1846), but the age-model can be extended given the lack of sedimentary variations to the core bottom. Therefore, a constant MAR of 2.3 kg·m^{-2}·year^{-1} allows the dating of the core base at approximately 1778 ± 11 years. This result is consistent with the previously mentioned morphodynamic evolution of the floodplain and, therefore, the UWC can be considered as a complete sequence of fine-grained aggradation.

For RBC, accurate dating based on a constant rate of accumulation between two date-bounded lacks may be less robust because there is no linear accretion caused by erosional processes controlling the river bank vertical accretion. Without considering this limit, the MAR reaches 2.4 kg·m^{-2}·year^{-1} between the 1933 and 2012 time markers. During this period, the MAR varies a maximum of 12.5% of this value, which induces an associated error of 4 years (Fig. 3). To date the 28–144 cm sequence, we correlated the base of the two archives at approximately 1778 ± 11 years and defined this date to be the beginning of fine-grained aggradation. In this sequence, the MAR reaches 6.2 kg·m^{-2}·year^{-1} with a maximum error of ±11 years.

The proximal floodplain aggradation in the RBC, which lasted at least from the 1760s to the late 1770s, has a MAR of 17.4 kg·m^{-2}·year^{-1}, materializing an important sediment transport at the end of the LIA and a MAR gradient from the proximal to distal floodplain. A similar spatial variability was shown by Walling and He (1998) at a floodplain scale.

For fine-grained sedimentation, MARs estimated over the 234 years for the two archives (4.9 kg·m^{-2}·year^{-1} for RBC and 2.0 kg·m^{-2}·year^{-1} for UWC) are comparable with values generally calculated in floodplains (*e.g.*, 1.0 to 6.6 kg·m^{-2}·year^{-1} by Walling and He, 1997; 0.7 to 5.9 kg·m^{-2}·year^{-1} by He and Walling, 1996). In this study, the MAR is more than 2 times larger for the RBC than for UWC (3 times larger for cum). During overbank floods, important differences of sediment deposition rates exist between morphological units at the floodplain scale, not necessarily correlated to ground-level elevation (Baborowski et al., 2007). Walling and He (1997, 1998) explained that the large MAR variability detected in distal floodplains is usually controlled by connection degree variations (with the river channel) rather than topographical forcing. Natural depressions, such as paleochannels, do not necessarily have the highest accumulation rates because their connectivity with the main channel limits fine-grained deposition compared to their outer margins. During overbank floods, sediment deposition is less important in the UWC than the RBC because transported sediments are evacuated by the downstream connection before settling. However, stored sediments are better preserved long-term in the paleochannel than in a river bank.

During the archived period, the MAR is not constant for the two cores. The Decize Dam elevation in 1933 moderates the MAR by 44% in the UWC and even more in the RBC (−68%), highlighting the dramatic reduction of overbank inputs for the river bank. The reduction in the magnitude and the frequency of overbank floods, or/and decline of transported sediment recorded since the 19th century and the second part of the 20th century in many anthropized rivers, can explain this trend (Owens et al., 1999; Arnaud-Fassetta, 2003; Benedetti, 2003; Lecce and Pavlowsky, 2004; Du and Walling, 2012).
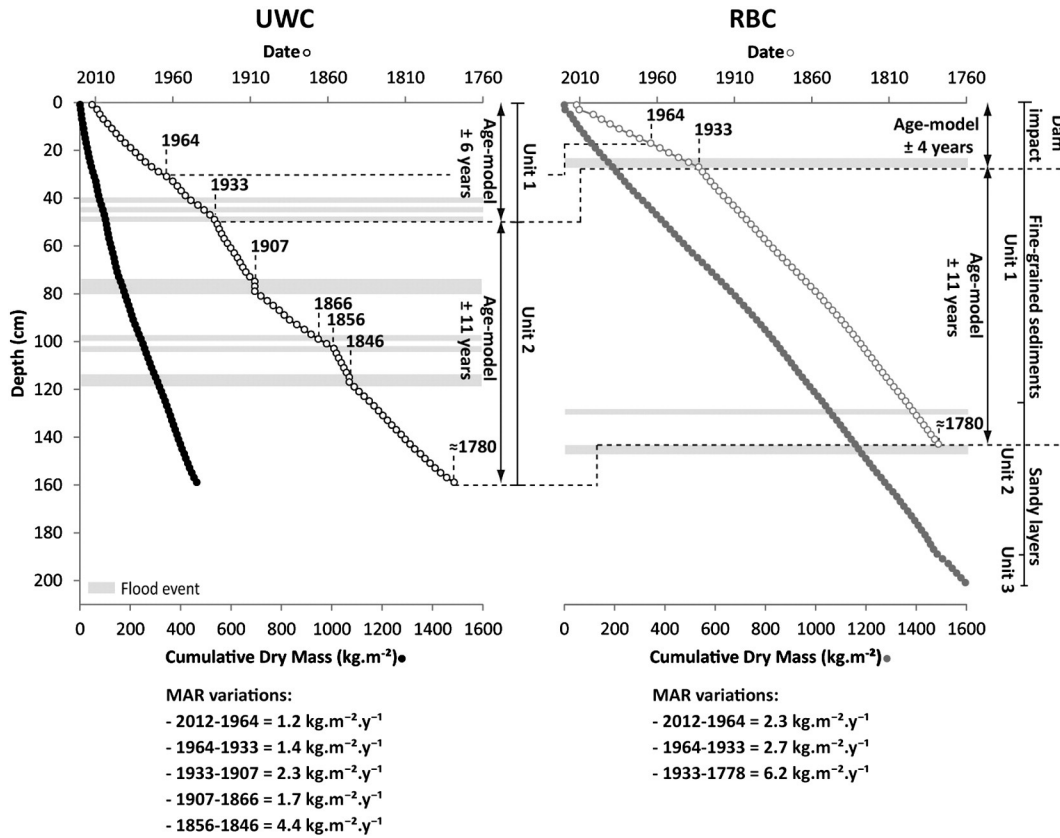
Fig. 3. Time correlation, age model definition and mass accumulation rates temporal variations in the two cores.

3.3. Influences of archiving processes on geochemical patterns

3.3.1. Comparison of the local geochemical background in fluvial environments

Depositional environments influence sediment texture and aggradation rate, but can they control geochemical composition? For the sandy Loire River, variations of Si/Al ratios and some Rare Earth Elements (REE), such as Hf and Sm concentrations, can be used as tracers of silico-clastic and heavy mineral inputs, even in the <63 μm fraction (Dhivert et al., in press).

In this study, Si/Al ratios and Hf concentrations are significantly correlated in both cores ($r = 0.9$, $p < 0.05$, $n = 181$). However, significant differences in their geochemical profiles are observed between sediments deposited in the proximal floodplain (126–202 cm in the RBC) and those archived in the distal floodplain (0–126 cm for the RBC and 50–160 cm before the dam elevation of 1933 for the UWC; Fig. 4, Tables 1 and 2).

During proximal floodplain aggradation (only in the RBC), Si/Al ratios and Hf concentrations have the maximum values of all profiles and are highly variable (Fig. 4). Si/Al ratios and Hf concentrations decrease from the bottom to 126 cm according to a fining upward trend ($r = 0.6$, $p < 0.05$, $n = 33$ with D_{50}). In this dynamic environment, sediments (essentially sands) are mainly composed of Si-rich detrital particles and REE-rich heavy minerals.

During distal floodplain aggradation, both cores have lower Si/Al ratios and Hf concentrations with much smaller variations than in the proximal floodplain (Fig. 4). Sediments are poorer in Si-rich sands and REE-rich heavy particles in favor of fine-grained sediments, and richer in Al. Additionally, for the UWC, the 0–50 cm sediment layers, deposited after 1933, have Si/Al ratios and Hf concentrations similar to the proximal floodplain environment of the RBC (Fig. 4). The 0–50 cm levels are coarser compared to sediments archived below because of slackwater deposition of fine sands after the elevation of the dam.

The sandy fraction of the Loire River sediments mobilized during high discharge events are composed of Si-rich minerals, such as quartz and REE-rich heavy minerals. In the fining upward sequence recorded in the proximal floodplain, (Si, REE)-rich sands are less present. This is the result of a bottom-up decreasing trend of the depositional environment energy. A progressive disconnection of the river bank induces a change in the grain size and mineralogical composition. However, fine-grained sediments settled in a low-energy distal floodplain in a highly disconnected environment with a homogenous mineralogical composition. After the dam elevation, the connection degree enhanced in the UWC, and the sandy fraction composed of (Si, REE)-rich minerals are more expressively represented.

These results highlight a high variability of detrital material input, influencing the mineralogical and the geochemical signature across a floodplain, even in the <63 μm fraction. The mineral distribution depends on the connection degree in the depositional environment.

Additionally, sediments deposited during the preindustrial period allows for the definition of natural TE concentrations specific to the local geochemical background. In this study, these sediment layers can be used to highlight the influences of depositional environments on measured preindustrial concentrations. Therefore, sediments older than the 1830s (100–202 cm for the RBC; 128–160 cm for the UWC) are considered. The background levels could have been affected by the first coal mining activities in the upstream basin (Woronoff, 1994, French coal mining agency, 2013).

In the distal floodplain environment, Al concentrations and TE concentrations are very similar along both cores (Table 3). The two cores have similar concentrations with median differences less than 11% for all of the cited TE. No significant differences in TE distributions ($p > 0.05$, $n = 28$) were noted, except for Pb and U. Therefore, the local geochemical background can be well-defined in this highly disconnected context because the mineralogical composition of settled fine-
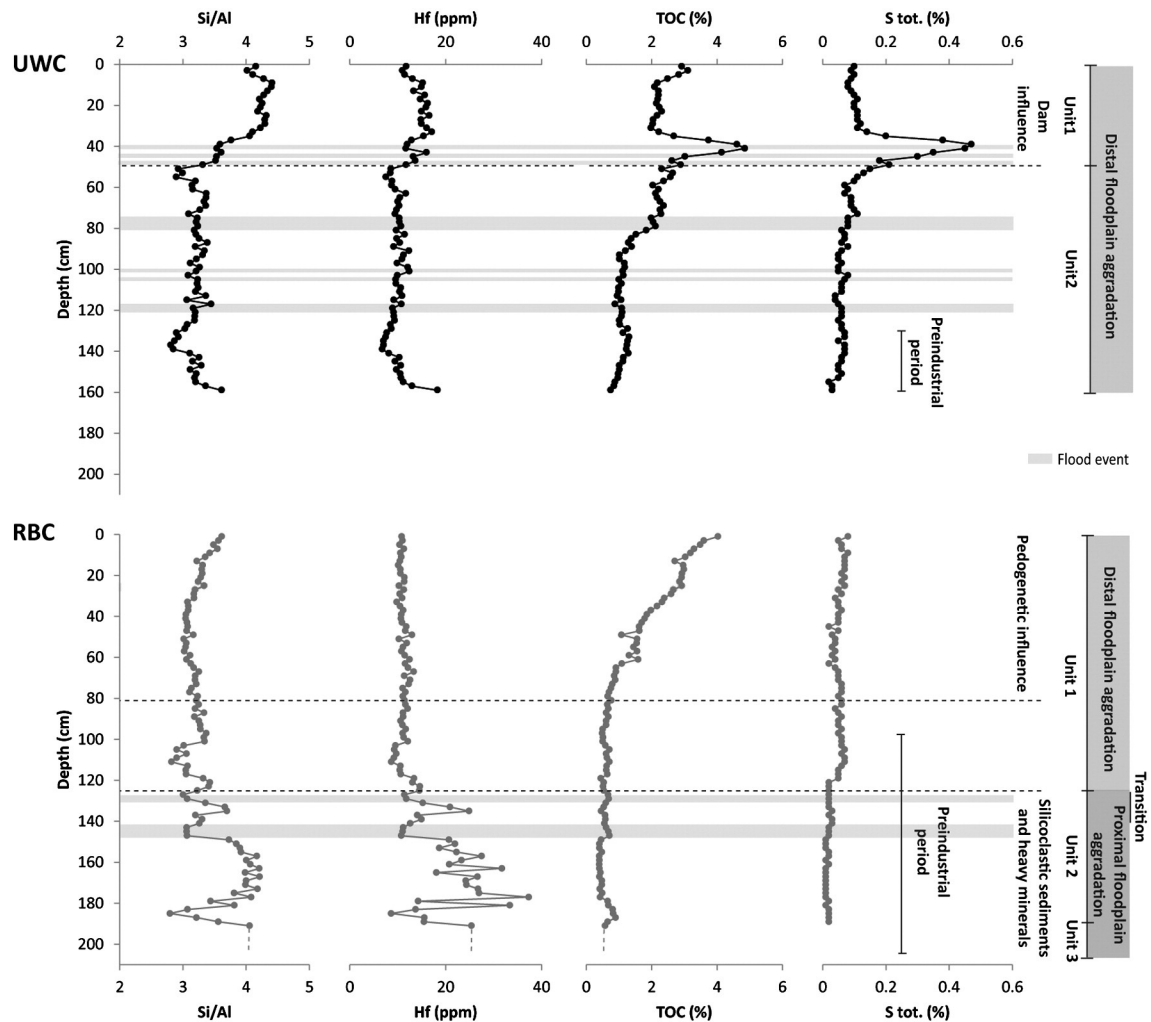
Fig. 4. Vertical profiles of Si/Al ratio, Hf, TOC and S concentrations for the two cores.

grained sediments is homogenous across the distal floodplain and stable over the registered period.

In the proximal floodplain sequence (only in the RBC), the chemical composition is more variable than in the distal floodplain (Table 3). This can be related to the mineralogical sorting associated with river bank accretion. This process results in accumulated sediments during overbank floods. However, the geochemical compositions of deposited sediments in the proximal floodplain depend on flood magnitudes and river morphology (Birch et al., 2001; Martin, 2000). Considering the influence of the energetic gradient on particle mineralogy and induced chemical variability in the proximal floodplain sequence, measured geochemical backgrounds are less representative than in the distal environment. Distributions of TE concentrations measured in the proximal floodplain are significantly different from those in the distal floodplain ($p < 0.05$, $n = 61$, except for Cr and Ni). However, TE concentrations are in the same range of magnitude in both depositional environments, except for Cd, U, Hg and, to a lesser extent, Sn. They present over-ranges of 77%, 111%, 65%, and 52%, respectively, compared to the distal floodplain maximum. The differences between the two depositional environments could be related to mineralogical sorting from the proximal to distal floodplain. Cd and U are significantly correlated to Hf concentrations ($r = 0.9$, $p < 0.05$, $n = 61$). Cadmium and U enrichments in the proximal floodplain sediments can be explained by a higher percentage of their heavy mineral hosts in the sandy fraction, i.e., zircons, barites, phosphorites and Ti-bearing heavy minerals (Dill, 2010).

Intra-site variability of natural TE concentrations exists at a local scale between sediments deposited in the proximal and the distal

floodplain, but what do they represent when compared with inter-site differences? To answer this question, the defined local background concentrations can be compared to preindustrial TE levels in fine-grained sediments archived at the most downstream station of the basin (Grosbois et al., 2012) and are representative of an average background at the entire Loire Basin scale (Table 3). Enrichment factors (EF) were calculated using the double normalization of Al contents and the preindustrial TE levels. For Bi, Cr, Cu, Ni, Sn, U, W and Zn, the EFs are close to 1 for deposited sediments in both distal and proximal floodplain environments. The local geochemical background for this TE is then similar to the one assumed for the basin. For Cd and U unit, EFs are verified in the distal environment, but have significant differences in the proximal environment ($p < 0.05$, $n = 61$, EF ranged between 1 and 4 for Cd, 1 and 3 for U). In the Loire Basin, the mineralogical variability linked to proximal environment dynamics induces larger geochemical variations in the Cd and U concentrations than the upstream–downstream gradient because of heavy mineral relative abundances. For distal and proximal environments, As, Hg, Mo and Sb have light enrichments in sedimentary levels older than the 1830s (EF ranged between 1 and 6). Preindustrial Hg concentrations in the UWC and the RBC are low and similar to those archived in the downstream part of the Loire Basin. The reason for Hg enrichments is not significant (Table 3). However, for As, Mo and Sb, enrichments can be related to a local geochemical anomaly 50 km upstream of the study station, associated with Variscan hydrothermal mineralization, which could provide (As–Mo–Sb)-rich chalcopyritic bearing phases (Delfour et al., 1984).

Table 3

Geochemical composition of preindustrial sediments (<1830) in the paleochannel (UWC) and river bank (RBC) cores compared to preindustrial concentrations representative of the all-natural sources at the entire Loire Basin scale (*Grosbois et al., 2012) and prehistorical concentrations in organic sediments of the Upper Loire Basin (** ARTEHIS — UMR 6298 — Dijon University, France). n.d. = not determined; Med. = Median value; Var. = Range variability compare to the median value; Unit: Si, Al, TOC, S tot. (%); As, Bi, Cd, Cr, Cu, Hg, Mo, Ni, Pb, Sb, Sn, U, W, Zn (ppm).

	UWC — distal floodplain (n = 15)			RBC — distal floodplain (n = 13)			RBC — proximal floodplain (n = 33)			Entire Loire Basin (n = 2)*		Upper Loire Basin (n = 1)** <6000 BP
	Range	Med.	Var.	Range	Med.	Var.	Range	Med.	Var.			
Si	26.4–28.4	27.30	7	26.0–28.5	27.10	9	25.5–31.3	29.60	20	n.d.	n.d.	20.34
Al	8.46–9.4	8.77	11	8.24–9.22	8.86	11	7.31–9.12	7.93	23	8.37	8.54	8.90
TOC	0.85–1.31	1.13	41	0.45–0.71	0.61	43	0.4–0.9	0.54	93	1.2	1.1	8.71
S tot.	0.02–0.07	0.06	83	0.02–0.07	0.06	83	0.01–0.03	0.02	100	n.d.	n.d	0.54
As	24.5–37.1	28.9	44	26.4–38	30.8	38	16.2–46.2	25.5	118	19.8	19.4	43.4
Bi	0.8–1.1	0.9	44	0.8–0.9	0.9	18	0.6–0.9	0.8	39	0.7	0.6	1.1
Cd	0.4–0.6	0.5	43	0.4–0.6	0.5	44	0.4–1.1	0.7	101	0.3	0.4	0.8
Cr	89–103	96	15	94–104	98	10	88–110	97	22	109	89	98
Cu	20.9–27.3	23.3	28	20.5–27.1	24.2	27	14.1–26.9	19.5	65	18.6	21.3	31.1
Hg	0.03–0.06	0.05	50	0.04–0.06	0.05	37	0.02–0.09	0.03	226	0.02	0.02	0.09
Mo	0.7–1.0	0.8	29	0.8–1.0	0.9	23	0.6–1.1	0.8	68	0.4	0.3	2.8
Ni	36.2–44.1	38.2	21	34.3–42.7	38.5	22	26.9–48.5	34.0	64	32.6	24.2	87.2
Pb	51–61	55	18	47–58	52	20	46–69	52	43	37.0	33	49
Sb	1.6–2.2	2.0	31	1.6–2.4	1.8	42	1.5–2.2	1.7	44	0.5	0.3	3.2
Sn	8–12	10	38	8–11	9	30	7–17	8	128	8	7	8
U	7.8–10.2	8.7	28	9.1–10.7	9.7	17	8.8–22.1	12.1	110	8.8	7.5	12.8
W	5.1–7.4	6.0	38	5.6–6.3	5.8	13	4.6–6.3	5.5	30	6.3	5.7	4.9
Zn	112–139	125	22	105–127	120	18	81–137	100	56	90	97	118

Because of the mineralogical sorting in the <63 μm fraction of floodplain sediments, the geochemical background measured in fine-grained sediments settled in the distal environment can be considered more representative of the basin scale. With the exception of specific local enrichments caused by geochemical anomalies, preindustrial concentrations in the upstream part of the Loire Basin are similar to those of the downstream basin. These results provide evidence for an average background reference at the basin scale and will be further used in this study.

3.3.2. Influence of archiving processes on anthropogenic TE variations

Archiving processes and associated connection degree variations influence sediment accumulation rates, major elements and natural TE levels. They can induce temporal discrepancies in anthropogenic TE variations. Because of this, archived TE temporal dynamics could be related to the sampling site choice. For the studied cores, do they allow access to a similar anthropogenic contamination history? This study focuses on distal floodplain sediments because proximal floodplain sediments are preindustrial with low to moderate enrichments of As, Cd, Mo, Sb, Sn and U, which are linked to mineralogical composition differences.

In the distal floodplain, the two cores have enrichment factors close to 1 for TEs up to the late 1860s, except for Hg, which has had a light enrichment (2 < EF < 4) since the 1850s (Fig. 5), and Sb and Mo which have higher geochemical backgrounds.

After the late 1860s, three different temporal dynamics are represented by Hg, Sn and Cd. First, a synchronic EF increase is calculated for Hg and Sn (up to 30 and 8, respectively) in both cores from the 1860s until the dam elevation in 1933. The other TE (Cd) shows EFs not higher than 2–3 (Fig. 5). Hg, and Sn profiles are different between the two cores. In the RBC, Hg enrichments gradually increase from the 1860s and reach a maximum of 21 in the 1930s. Sn enrichment becomes significant in the early 1900s and reaches a maximum of 7 in the late 1920s. In the UWC, TE enrichment profiles are different than in the RBC and characterize short temporal variations of contamination levels (Fig. 5). Hg enrichment sharply increases between the early 1880s and the early 1890s with a maximum EF of 30, higher than the RBC registered maximum. The Hg EF then decreases until the late 1900s (EF = 11, similar in RBC) before a second increase in the RBC (EF close to 23 in the early 1930s). For Sn, the EF profile is similar to the RBC variations with a light enrichment between the late 1900s and the early 1920s (EF = 4). However, this maximum EF peak is higher in the UWC

(EF = 10) than in the RBC. By the 1930s, enrichment levels are similar in both cores with maximum values higher in the UWC than in the RBC.

After the dam elevation in 1933, TE enrichment trends and maxima highly differ between the two cores. In the RBC, EF temporal trends significantly decrease for Hg and Sn (r = 0.8, p < 0.05, n = 14), reaching an enrichment level high for Hg in the early 2010s (EF = 11) and low for Sn (EF ca. 4). For Cd, the EF starts to increase with the dam elevation (EF ca. 3) and then remains stable (p > 0.05). In the UWC, the EF temporal trends are less linear than in the RBC. All of the studied TE have a period of maximum enrichment. The Hg maximum (EF ca. 57) occurred just after the dam elevation, between the early 1940s and the 1950s. The Sn maximum occurred (in the 1920s–1930s) before the dam elevation but the enrichment remains high until the 1940s (EF close to 8) and the Cd maximum occurs in the early 1950s (EF ca. 9). After these EF maxima, all of the TE enrichments slowly decrease, reaching enrichment levels less than those recorded in the RBC for Hg and Sn and similar for Cd.

These EF variations highlight the influence of settling environments on the archived anthropogenic TE history. In this studied floodplain and before water-depth control by the dam in the early 1930s, TE temporal trends are comparable in terms of trajectories and contamination levels, although the UWC has shorter-time variations and higher EF peaks. Even if the aggradation rate is higher for the RBC before 1933 (see Section 3.2.2), the temporal resolution of the recorded TE chronic is not as good as for the UWC. This is linked to a better conservative environment for the trapped sediments in the paleochannel.

After the dam elevation, differences in TE temporal dynamics are enhanced, with enrichments in UWC sediments becoming more variable and with higher EF peaks than in the RBC. The spatial variability of contamination levels in sediments deposited during overbank floods depends on the transport capacity of suspended materials (Baborowski et al., 2007). As a result of water-depth control, the aggradation rate of the RBC is largely reduced. Therefore, less potential contaminated particles can settle down in this part of the floodplain. Additionally, some organic particles containing a significant part of the total S and chalcophil TE-rich (such as As, Cd, Co, Cu, Hg, Mo, Ni, Sb, U and Zn, all highly correlated, r = 0.9, p < 0.05, n = 8) are trapped in the UWC between 34 and 50 cm and are absent in the RBC (Fig. 4). The dam elevation enhanced the connectivity degree for the UWC and archived conditions for these TE-rich particles compared to the RBC. These TOC-S increases could be related to metalliferous coal and blast furnace sludge activities in the
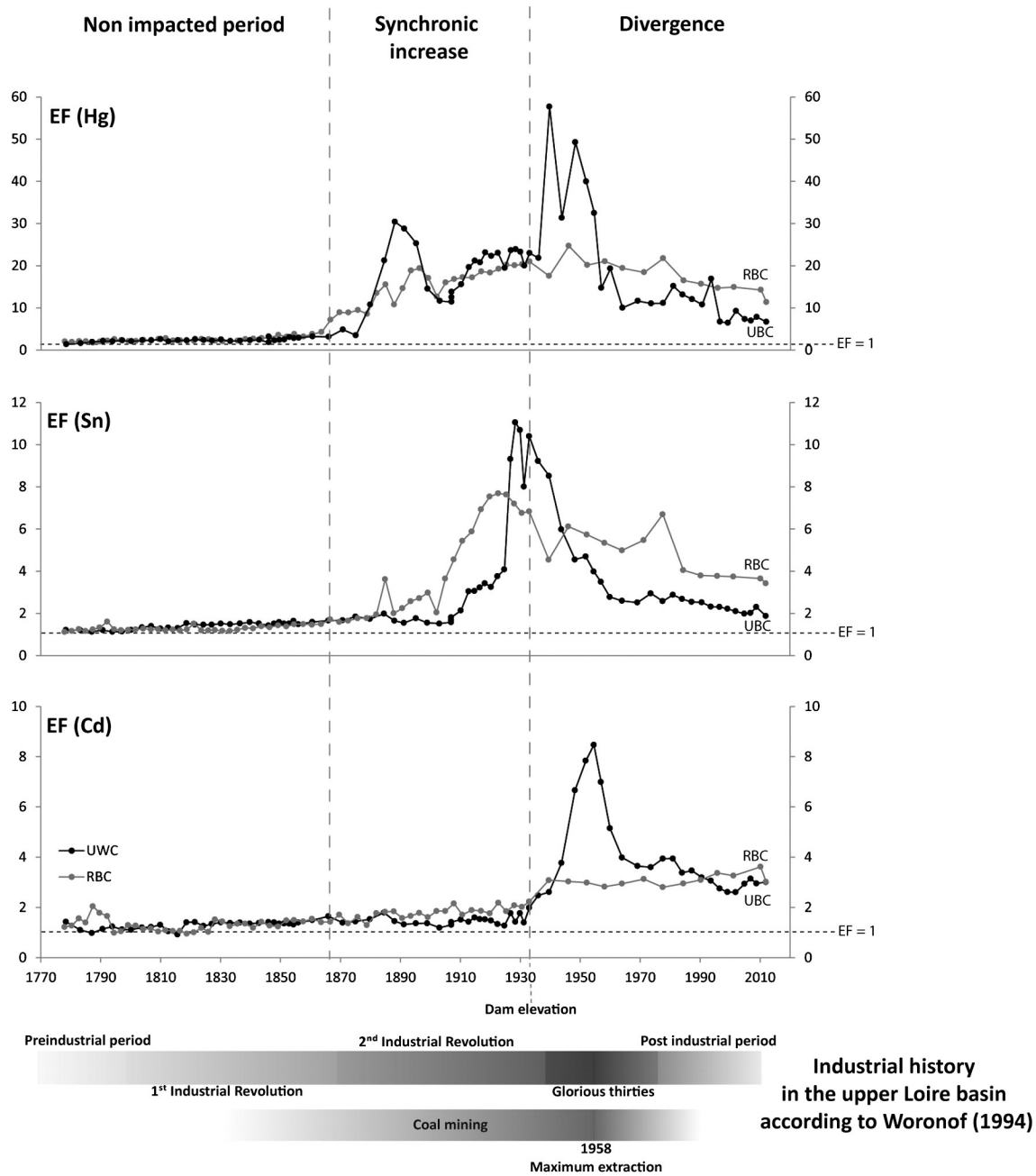
Fig. 5. Enrichment factor chronic of Hg, Sn and Cd for the two cores compared to the industrial history at the basin scale.

study area. Bioturbation, organic matter degradation and post-depositional processes can be important factors to explain differences in recorded TE chronics between the UWC and the RBC. The upper unit of the RBC, from 70 cm to the surface, has pedogenetic characteristics with secondary porosity, roots and a bottom-up important increase of TOC content (Fig. 4). TE-TOC correlations are significant in this core interval (r > 0.6, p < 0.05, n = 63). Surface sediments (post 1990s, <10 cm deep) of the RBC, and TOC-rich (>3%) with roots have higher contamination levels than the UWC. In a pedogenic context, the TE vertical distribution and contamination levels are more dependent on their high retention in surface because of an organic top soil and TE redistribution by biological activities than progressive archiving processes. These results have been shown by other authors (Palumbo et al., 2000; Fujikawa et al., 2000). At a long-term scale, this phenomenon should also be magnified by the high disconnection degree of the river bank and low sediment inputs induced by water depth control.

These results show a significant influence of the settling environment on archived long-term TE variations. In the paleochannel, TE temporal dynamics are archived with a well-defined time resolution and are not affected by connection degree variations. However, sediments cored in a river bank can be more influenced by river modifications and pedogenetic activities.

4. Conclusions

To highlight the influences of fluvial depositional environments on sediment archiving processes, aggradation rates and recorded geochemical patterns, two cores were sampled on a ridge of the river bank and in a paleochannel. In the river bank core, two steps of the floodplain edification are archived, corresponding to two successive depositional environments. The oldest one corresponds to a proximal floodplain sedimentation archived during the earliest age of the

floodplain during the end of the Little Ice Age. This sedimentary sequence shows a general fining upward sequence related to decreasing river energy during river bank accretion. Subsequently, a fine-grained material was homogenously settled during overbank floods to present day. Sediments in the underwater core of the paleochannel are similar to the upper unit of the river bank core. However, after the Decize dam elevation in 1933, slackwater depositions of fine sands have largely contributed to its aggradation.

The main differences between the two depositional environments highlighted in this study are

1. a better archiving capacity of sediments in a paleochannel as the river bank accretion is largely influenced by erosion episodes,
2. higher aggradation rates in the river bank, although more dependent on connection degree variations, with the aggradation rate significantly reduced after water depth regulation in this environment,
3. preindustrial geochemical concentrations are more dependent on river energy in proximal than distal areas because of the sorting of heavy minerals, and
4. in the paleochannel, trapped contaminated sediments are less selected and allow for a better time resolution of anthropogenic TE signals.

For this floodplain study, TE temporal dynamics archived in the paleochannel are more representative of an anthropogenic source history. However, TE temporal dynamics recorded in the river bank show similar trends than those of the paleochannel, with the divergences being caused by local water depth regulation and a biological redistribution of deposited TEs.

Acknowledgments

References

Arnaud-Fassetta G. River channel changes in the Rhone Delta (France) since the end of the Little Ice Age: geomorphological adjustment to hydroclimatic change and natural resource management. Catena 2003;51:141–72.

Bábek O, Hilscherová K, Nehyba S, Zeman J, Famera M, Francu J, et al. Contamination history of suspended river sediments accumulated in oxbow lakes over the last 25 years. J Soils Sediments 2008;8:165–76.

Bábek O, Faměra M, Hilscherová K, Kalvoda J, Dobrovolný P, Sedláček J, et al. Geochemical traces of flood layers in the fluvial sedimentary archive; implications for contamination history analyses. Catena 2011;87:281–90.

Babonaux Y. Le lit de la Loire - Etude d'hydrodynamique fluviale, vol. 2. Paris:Bibliothèque Nationale; 1970.

Baborowski M, Büttner O, Morgenstern P, Krüger F, Lobe I, Rupp H, et al. Spatial and temporal variability of sediment deposition on artificial-lawn traps in a floodplain of the River Elbe. Environ Pollut 2007;148:770–8.

Benedetti MM. Controls on overbank deposition in the Upper Mississippi River. Geomorphology 2003;56:271–90.

Berner ZA, Bleeck-Schmidt S, Stüben D, Neumann T, Fuchs M, Lehmann M. Floodplain deposits: a geochemical archive of flood history — a case study on the River Rhine, Germany. Appl Geochem 2012;27:543–61.

Birch GF, Taylor SE, Matthai C. Small-scale spatial and temporal variance in the concentration of heavy metals in aquatic sediments: a review and some new concepts. Environ Pollut 2001;113:357–72.

Bradley SB, Cox JJ. The significance of the floodplain to the cycling of metals in the river Derwent Catchment, U.K. Sci Total Environ 1990;97–98:441–54.

Bravard J-P, Peiry J-L. The CM pattern as a tool for the classification of alluvial suites and floodplains along the river continuum. In: Marrott SB, Alexander J, editors. Floodplains: interdisciplinary approaches, 163. Geol Soc Spec Publ; 1999. p. 259–68.

Bravard J-P, Goichot M, Tronchère H. An assessment of sediment-transport processes in the Lower Mekong River based on deposit grain sizes, the CM technique and flow-energy data. Geomorphology 2014;207:174–89.

Bridge J. Rivers and floodplains forms, processes, and sedimentary record. Blackwell Science Ltd.; 2003. p. 487.

Dacharry M. Hydrologie de la Loire en amont de Gien, 2Paris. N.A.L.; 1974 [334 & 285 pp.].

Cort De, Dubois G, Fridman SD, Germenchuk MG, Izrael Yu A, Janssens A. The atlas of caesium deposition on Europe after the Chernobyl accident. 16733. EUR: M. Luxembourg; 1998. ISBN 92-828-3140-X.

Charriau A, Lesven L, Gao Y, Leermakers M, Baeyens W, Ouddane B, Billon G. Trace metal behaviour in riverine sediments: Role of organic matter and sulfides. Appl Geochem 2011;26:80–90.

Delfour J, Isnard P, Lecuyer E, Lemiere B, Lhote F, Moine B, et al. Etude du gîte de pyrite de Chizeuil (Saône-et-Loire) et de son environnement volcano-sédimentaire dévonien et dinantien. Document BRGM, n° 73; 1984 [37 pp.].

Desmet M, Mourier B, Mahler BJ, Van Metre PC, Roux G, Persat H, et al. Spatial and temporal trends in PCBs in sediment along the lower Rhône River, France. Sci Total Environ 2012;433:189–97.

Détriché S, Rodrigues S, Macaire J-J, Bonté P, Bréhéret J-G, Bakyono J-P, et al. Caesium-137 in sandy sediments of the River Loire (France): assessment of an alluvial island evolving over the last 50 years. Geomorphology 2010;115:11–22.

Dhivert E, Grosbois C, Coynel A, Desmet M. Sedimentary and geochemical evidences in a core age model to highlight flood-event dynamics in a reservoir infill (Upper Loire basin, France). Catena 2014. [in press].

Dieras PL, Constantine JA, Hales TC, Piégay H, Riquier J. The role of oxbow lakes in the off-channel storage of bed material along the Ain River, France. Geomorphology 2013; 188:110–9.

Dill HG. The "chessboard" classification scheme of mineral deposits: mineralogy and geology from aluminum to zirconium. Earth Sci Rev 2010;100:1–420.

Du P, Walling DE. Using ^{210}Pb measurements to estimate sedimentation rates on river floodplains. J Environ Radioact 2012;103:59–75.

Euler T, Zemke J, Rodrigues S, Herguet J. Influence of inclination and permeability of solitary woody riparian plants on local hydraulic and sedimentary processes. Hydrol Process 2014;28:1358–71.

Ferrand E, Eyrolle F, Radakovitch O, Provansal M, Dufour S, Vella C, et al. Historical levels of heavy metals and artificial radionuclides reconstructed from overbank sediment records in lower Rhône River (South-East France). Geochim Cosmochim Acta 2012; 82:163–82.

Förstner U, Heise S, Schwartz R, Westrich B, Ahlf W. Historical contaminated sediments and soils at the river basin scale. J Soils Sediments 2004;4:247–60.

Fujikawa Y, Fukui M, Kudo A. Vertical distributions of trace metals in natural soil. Water Air Soil Pollut 2000;123:1–21.

Fuller IC. Geomorphic impacts of a 100-year flood: Kiwitea Stream, Manawatu catchment, New Zealand. Geomorphology 2008;98:84–95.

Gasowski Z. L'enfoncement du lit de la Loire/The entrenchment of the Loire's river bed. Rev Géogr Lyon 1994;69:41–5.

Gocht T, Moldenhauer K, Pu W. Historical record of polycyclic aromatic hydrocarbons (PAH) and heavy metals in floodplain sediments from the Rhine River (Hessisches Ried, Germany). Appl Geochem 2001;16:1707–21.

Grivel S, Gautier E. Mise en place des îles fluviales en Loire moyenne, du 19e siècle à aujourd'hui. Cybergeo Eur J Geogr 2012;615.

Grosbois C, Meybeck M, Lestel L, Lefèvre I, Moatar F. Severe and contrasted polymetallic contamination patterns (1900–2009) in the Loire River sediments (France). Sci Total Environ 2012;435–436:290–305.

Grousset FE, Jouanneau JM, Castaing P, Lavaux G, Latouche C. A 70 year record of contamination from industrial activity along the Garonne River and its tributaries (SW France). Estuar Coast Shelf Sci 1999;48:401–14.

Grygar T, Světlík I, Lisá L, Koptíková L, Bajer A, Wray DS, et al. Geochemical tools for the stratigraphic correlation of floodplain deposits of the Morava River in Strážnické Pomoraví, Czech Republic from the last millennium. Catena 2010; 80:106–21.

Grygar MT, Elznicová J, Bábek O, Hošek M, Engel Z, Kiss T. Obtaining isochrones from pollution signals in a fluvial sediment record: a case study in a uranium-polluted floodplain of the Ploučnice River, Czech Republic. Appl Geochem 2014. [in press].

He Q, Walling DE. Interpreting particle size effects in the adsorption of 13' Cs and unsupported 210Pb by mineral soils and sediments. Earth Surf Process Landf 1996;30: 117–37.

Heaven S, Ilyushchenko MA, Tanton TW, Ullrich SM, Yanin EP. Mercury in the River Nura and its floodplain, Central Kazakhstan: I. River sediments and water. Sci Total Environ 2000;260:35–44.

Hoffmann T, Thorndycraft VR, Brown AG, Coulthard TJ, Damnati B, Kale VS, et al. Human impact on fluvial regimes and sediment flux during the Holocene. Rev Futur Res Agenda Glob Planet Chang 2010;72:87–98.

Hostache R, Hissler C, Matgen P, Guignard C, Bates P. A 2-D hydro-morphodynamic modelling approach for predicting suspended sediment propagation and related heavy metal contamination in floodplain: a sensitivity analysis. Hydrol Earth Syst Sci Discuss 2014;11:1741–76.

Houben P. Geomorphological facies reconstruction of Late Quaternary alluvia by the application of fluvial architecture concepts. Geomorphology 2007;86:94–114.

Hughes AO, Croke JC, Pietsch TJ, Olley JM. Changes in the rates of floodplain and in-channel bench accretion in response to catchment disturbance, central Queensland, Australia. Geomorphology 2010;114:338–47.

Knox JC. Floodplain sedimentation in the Upper Mississippi Valley: natural versus human accelerated. Geomorphology 2006;79:286–310.

Landon N. L'évolution contemporaine du profil en long des affluents du Rhône moyen. Constat régional et analyse d'un hydrosystème complexe, la Drôme, Paris; 1999. p. 560.

Latapie A. Modélisation de l'évolution morphologique d'un lit alluvial: application à la Loire moyenne. PhD thesis Tours Univ.; 2011 [277 pp.].

Latapie A, Camenen B, Rodrigues S, Paquier A, Bouchard JP, Moatar F. Assessing channel response of a long river influenced by human disturbance. Catena 2014;121:1–12.

Le Cloarec M-F, Bonte PH, Lestel L, Lefèvre I, Ayrault S. Sedimentary record of metal contamination in the Seine River during the last century. Phys Chem Earth A/B/C 2011; 36:515–29.

Lecce SA, Pavlowsky RT. Storage of mining-related zinc in floodplain sediments, Blue River, Wisconsin. Phys Geogr 1997;18:424–39.

Lecce SA, Pavlowsky RT. Spatial and temporal variations in the grain-size characteristics of historical flood plain deposits, Blue River, Wisconsin, USA. Geomorphology 2004;61: 361–71.

Lecce SA, Pavlowsky RT. Floodplain storage of sediment contaminated by mercury and copper from historic gold mining at Gold Hill, North Carolina, USA. Geomorphology 2014;206:122–32.

Leteinturier B, Engels P, Petit F, Chiffaut A, Malaisse F. Morphodynamisme d'un tronçon de Loire bourbonnaise depuis le XVIIIe siècle/changing dynamics of the Loire river in Burgundy (France) during the last 200 years. Géomorphologie: relief, processus, environnement, 4. 2000. p. 239–51.

Macaire JJ, Gay-Ovejero I, Bacchi M, Cocirta C, Patryl L, Rodrigues S. Petrography of alluvial sands as a past and present environmental indicator: case of the Loire River (France). Int J Sediment Res 2013;28:285–303.

Macklin MG, Klimek K. Dispersal, storage and transformation of metal contaminated alluvium in the upper Vistula basin, southwest Poland. Appl Geogr 1992;12:7–30.

Martin CW. Heavy metal trends in floodplain sediments and valley fill, River Lahn, Germany. Catena 2000;39:53–68.

Matisoff G, Ketterer ME, Rosén K, Mietelski JW, Vitko LF, Persson H, et al. Downward migration of Chernobyl-derived radionuclides in soils in Poland and Sweden. Appl Geochem 2011;26:105–15.

Meitzen KM, Doyle MW, Thoms MC, Burns CE. Geomorphology within the interdisciplinary science of environmental flows. Geomorphology 2013;200:143–54.

Mourier B, Desmet M, Van Metre PC, Mahler BJ, Perrodin Y, Roux G, et al. Historical records, sources, and spatial trends of PCBs along the Rhône River (France). Sci Total Environ 2014;476–477:568–76.

Nanson GC, Croke JC. A genetic classification of floodplains. Geomorphology 1992;4: 459–86.

Nanson GC, Page K. Lateral accretion of fine-grained concave benches on meandering rivers. In: Collinson JD, Lewin J, editors. Modern and Ancient Fluvial Systems. Blackwell Publishing Ltd.; 1983

Owens PN, Walling DE, Leeks GJL. Use of floodplain sediment cores to investigate recent historical changes in overbank sedimentation rates and sediment sources in the catchment of the River Ouse, Yorkshire, UK. Catena 1999;36:21–47.

Palumbo B, Angelone M, Bellanca A, Dazzi C, Hauser S, Neri R, et al. Influence of inheritance and pedogenesis on heavy metal distribution in soils of Sicily, Italy. Geoderma 2000;95:247–66.

Passega R. Texture as characteristic of clastic deposition. Bull Am Assoc Pet Geol 1957;41: 1952–84.

Passega R. Grain-size representation by CM pattern as a geological tool. J Sediment Petrol 1964;34:830–47.

Pye K, Blott SJ. Particle size analysis of sediments, soils and related particulate materials for forensic purposes using laser granulometry. Forensic Sci Int 2004;144:19–27.

Rodrigues S, Bréhéret J-G, Macaire J-J, Moatar F, Nistoran D, Jugé P. Flow and sediment dynamics in the vegetated secondary channels of an anabranching river: the Loire River (France). Sediment Geol 2006;186:89–109.

Rodrigues S, Breheret J-G, Macaire J-J, Greulich S, Villar M. In-channel woody vegetation controls on sedimentary processes and the sedimentary record within alluvial environments: a modern example of an anabranch of the River Loire (France). Sedimentology 2007;54:223–42.

Schulz-Zunkel C, Krueger F, Rupp H, Meissner R, Gruber B, Gerisch M, et al. Spatial and seasonal distribution of trace metals in floodplain soils. A case study with the Middle Elbe River, Germany. Geoderma 2013;211:128–37.

Thompson C, Croke J. Geomorphic effects, flood power, and channel competence of a catastrophic flood in confined and unconfined reaches of the upper Lockyer valley, southeast Queensland, Australia. Geomorphology 2013;197:156–69.

Valverde L, Jugé P, Handfus T. Résultats granulométriques et localisation des points dures en Loire. rapport InfoSed, 2. 2; 2013. p. 180.

van Griethuysen C, Luitwieler M, Joziasse J, Koelmans AA. Temporal variation of trace metal geochemistry in floodplain lake sediment subject to dynamic hydrological conditions. Environ Pollut 2005;137:281–94.

Van Metre PC, Wilson JT, Fuller CC, Callender E, Mahler BJ. Collection, analysis, and age-dating of sediment cores from 56 U.S. lakes and reservoirs sampled by the U.S. gological survey. 1992–2001 USGS Scientific Investigations Report, 5184. 2004.

Vrel A, Boust D, Lesueur P, Deloffre J, Dubrulle-Brunaud C, Solier L, et al. Dating of sediment record at two contrasting sites of the Seine River using radioactivity data and hydrological time series. J Environ Radioact 2013;126:20–31.

Walling DE, He Q. Use of fallout ^{137}Cs in investigations of overbank sediment deposition on river floodplains. Catena 1997;29:263–82.

Walling DE, He Q. The spatial variability of overbank sedimentation on river floodplains. Geomorphology 1998;24:209–23.

Walling DE, Owens PN, Leeks GJL. The characteristics of overbank deposits associated with a major flood event in the catchment of the River Ouse, Yorkshire, UK. Catena 1997;31:53–75.

Walling DE, Owens PN, Leeks GJL. The role of channel and floodplain storage in the suspended sediment budget of the River Ouse, Yorkshire, UK. Geomorphology 1998;22:225–42.

Werritty A, Paine JL, Macdonald N, Rowan JS, McEwen LJ. Use of multi-proxy flood records to improve estimates of flood risk: Lower River Tay, Scotland. Catena 2006;66: 107–19.

Woronoff D. Histoire de l'industrie en France, Du 16e siècle à nos jours, Paris. Le Seuil; 1994 [671 pp.].